Article

Developmental Cell

Secreted PTEN binds PLXDC2 on macrophages to drive antitumor immunity and tumor suppression

Graphical abstract

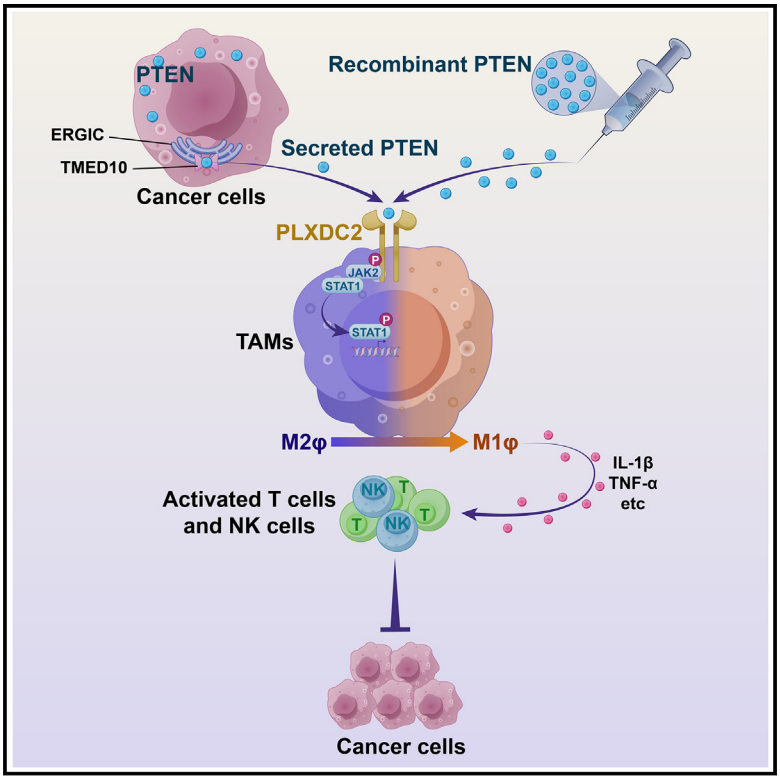

Authors

Cheng Zhang, Hong-Ming Ma, Shuai Wu, ..., Jun-Ke Zheng, Guo-Qiang Chen, Shao-Ming Shen

Correspondence

chengq@shsmu.edu.cn (G.-Q.C.), smshen@shsmu.edu.cn (S.-M.S.)

In brief

Zhang et al. show that PTEN is secreted as a soluble protein by the TMED10-mediated unconventional protein secretion pathway into the extracellular space, where it exerts a cytokine-like role by binding with PLXDC2 on macrophages to sequentially activate JAK2-STAT1 signaling, reprogram macrophages, and drive antitumor immunity.

Highlights

- PTEN is secreted via the TMED10-channeled protein secretion pathway
- Cytokine-like PTEN binds with its receptor PLXDC2 on macrophages
- PTEN-PLXDC2 engagement drives antitumor immunity by reprogramming macrophages
- Extracellular PTEN synergizes with PD-1 blockade to suppress tumor growth

Zhang et al., 2024, Developmental Cell *59*, 1–17
December 2, 2024
https://doi.org/10.1016/j.devcel.2024.08.003

CellPress

Developmental Cell

CellPress

Article

Secreted PTEN binds PLXDC2 on macrophages to drive antitumor immunity and tumor suppression

Cheng Zhang,[1,2,4] Hong-Ming Ma,[1,3,4] Shuai Wu,[3,4] Jia-Ming Shen,[1,3,4] Na Zhang,[3] Yi-Lu Xu,[3] Cheng-Xiao Li,[3] Ping He,[1] Meng-Kai Ge,[3] Xi-Li Chu,[3] Yu-Xue Zhang,[3] Jun-Ke Zheng,[3] Guo-Qiang Chen,[1,2,*] and Shao-Ming Shen[1,3,5,*]

[1]Institute of Aging & Tissue Regeneration, Stress and Cancer Research Unit of Chinese Academy of Medical Sciences (No.2019RU043), State Key Laboratory of Systems Medicine for Cancer, Ren-Ji Hospital, Shanghai Jiao Tong University School of Medicine (SJTU-SM), Shanghai 200127, China

[2]School of Basic Medicine and Life Science, Hainan Academy of Medical Sciences, Hainan Medical University, Haikou, Hainan 571199, China

[3]Department of Pathophysiology, Key Laboratory of Cell Differentiation and Apoptosis of Chinese Ministry of Education, SJTU-SM, Shanghai 200025, China

[4]These authors contributed equally

[5]Lead contact

*Correspondence: chengq@shsmu.edu.cn (G.-Q.C.), smshen@shsmu.edu.cn (S.-M.S.)

https://doi.org/10.1016/j.devcel.2024.08.003

SUMMARY

Loss of phosphatase and tensin homolog (PTEN) has been linked to an immunosuppressive tumor microenvironment, but its underlying mechanisms remain largely enigmatic. Here, we report that PTEN can be secreted by the transmembrane emp24 domain-containing protein 10 (TMED10)-channeled protein secretion pathway. Inhibiting PTEN secretion from tumor cells contributes to immunosuppression and impairs the tumor-suppressive role of PTEN, while intratumoral injection of PTEN protein promotes antitumor immunity and suppresses tumor growth in mice. Mechanistically, extracellular PTEN binds to the plexin domain-containing protein 2 (PLXDC2) on macrophages, triggering subsequent activation of JAK2-STAT1 signaling, which switches tumor-associated macrophages (TAMs) from the immunosuppressive to inflammatory phenotype, leading to enhanced activation of $CD8^+$ T and natural killer cells. Importantly, PTEN treatment also enhances the therapeutic efficacy of anti-PD-1 treatment in mice and reverses the immune-suppressive phenotype of patient-derived primary TAMs. These data identify a cytokine-like role of PTEN in immune activation and tumor suppression and demonstrate the therapeutic potential for extracellular administration of PTEN in cancer immunotherapy.

INTRODUCTION

Phosphatase and tensin homolog on chromosome 10 (PTEN) is one of the tumor suppressors most frequently inactivated in human cancer.[1,2] Even a partial loss of its function (haploinsufficiency) may cause neoplastic transformation.[2–4] The most extensively studied tumor-suppressive function of PTEN is its lipid phosphatase activity, which antagonizes the phosphatidylinositol-3-kinase (PI3K) signaling, whereas it is now well recognized that its protein phosphatase activity as well as phosphatase-independent activities also contribute to the tumor-suppressive function of PTEN.[2,5] Several therapeutic approaches are currently being explored to combat PTEN-deficient tumors. Besides, more and more efforts are being put into approaches aiming to restore PTEN function, although it is thought to be presently not feasible.[6,7]

Cancer cells can co-evolve with the tumor immune microenvironment (TIME) to develop different strategies to evade T cell immune destruction, and it is a critical effort to dissect the links between oncogenic processes and immune evasion. PTEN loss has been reported to promote immune suppression and therapeutic resistance to immunotherapy in various cancer types, including melanoma, uterine leiomyosarcoma, prostate tumors, glioma, and invasive breast cancer,[8–12] in which PI3K-AKT or PI3Kβ-signal transducer and activator of transcription 3 (STAT3) signaling have been shown to play mediating roles.[8,11] Thus, current evidence suggests that immune evasion upon PTEN loss is an indirect secondary consequence of PI3K signaling dysregulation. However, whether PTEN regulates tumor immunity in a direct way is unknown.

Here, we report that PTEN is secreted via the transmembrane emp24 domain-containing protein 10 (TMED10)-channeled unconventional protein secretion (UPS) pathway into the extracellular space, where it binds plexin domain-containing protein 2 (PLXDC2) expressed on the surface of macrophages. The engagement of PLXDC2 by PTEN reprograms macrophages in the tumor microenvironment (TME) toward a proinflammatory phenotype, thus promoting antitumor immune responses and tumor suppression. These findings dissect the mechanism of PTEN loss-caused immunosuppression by identifying a

Please cite this article in press as: Zhang et al., Secreted PTEN binds PLXDC2 on macrophages to drive antitumor immunity and tumor suppression, Developmental Cell (2024), https://doi.org/10.1016/j.devcel.2024.08.003

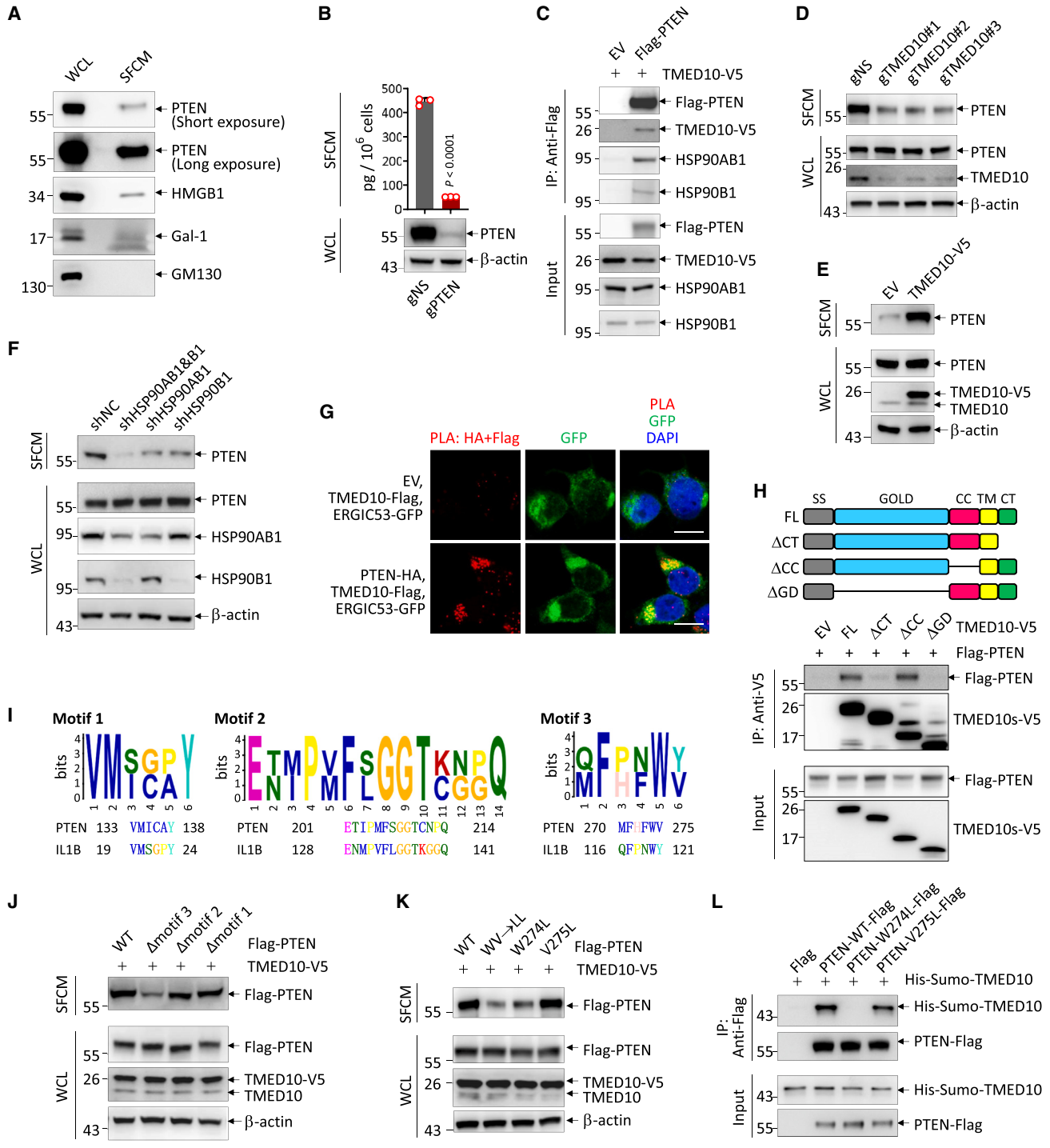

Figure 1. PTEN is secreted via the TMED10-channeled unconventional protein secretion pathway

(A) Western blot (WB) analysis of the indicated proteins in SFCM (serum-free conditioned medium) and WCL (whole-cell lysate) of 293T cells.

(B) ELISA of PTEN in SFCM of 293T cells transduced with gNS or gPTEN (n = 3).

(C) Anti-FLAG co-immunoprecipitation (coIP) in 293T-ΔPTEN cells co-transfected with TMED10-V5 and empty vector (EV) or FLAG-PTEN.

(D–F) WB analysis of secreted PTEN in 293T cells transduced with gNS or gTMED10 (D), transfected with EV or TMED10-V5 (E), and transduced by the indicated shRNAs (F).

(G) Duolink PLA assay for PTEN-HA and TMED10-FLAG in ERGIC53-GFP-expressing 293T-ΔPTEN cells transfected with the indicated plasmids (scale bars, 10 μm).

(H) Anti-V5 coIP in 293T-ΔPTEN cells co-transfected with FLAG-PTEN and the indicated TMED10-V5 variants.

(I) Homologous motifs predicted by MEME in PTEN and IL-1β.

(legend continued on next page)

Please cite this article in press as: Zhang et al., Secreted PTEN binds PLXDC2 on macrophages to drive antitumor immunity and tumor suppression, Developmental Cell (2024), https://doi.org/10.1016/j.devcel.2024.08.003

cytokine-like role of PTEN and provide an avenue to restore PTEN function by treating cancer directly with PTEN protein.

RESULTS

Soluble PTEN is secreted via the TMED10-channeled protein secretion pathway

We surprisingly found PTEN protein in the culture supernatants of various cell lines, along with other known secretory proteins such as high mobility group protein B1 (HMGB1) and galectin-1 (Gal-1) (Figures 1A and S1A). The absence of Golgi-localized protein 130 kDa *cis*-Golgi matrix protein (GM130) in the supernatant of 293T cells excluded that the PTEN protein in supernatants was from dead cells (Figure 1A). On the other hand, supernatants collected from PTEN-knockout mouse embryonic fibroblasts (MEFs) and PTEN-deficient U251 glioblastoma cells showed no detectable PTEN (Figure S1A), supporting that the PTEN protein in the culture supernatants of PTEN-intact cells is cells-derived. Quantification with enzyme-linked immunosorbent assay (ELISA) revealed that one million 293T cells secreted ~450 pg of PTEN protein into the medium during 1 h's incubation, whereas knockout of PTEN by guide RNA (gRNA)-directed CRISPR-Cas9 system eliminated it (Figure 1B). These data indicate that intracellular PTEN protein is secreted into the extracellular space.

Considering that PTEN was reported to be exported via exosome,[13] we addressed the possibility of exosome-mediated secretion of PTEN. For this purpose, medium incubated with 293T cells for 1 or 24 h was collected and subjected to exosome isolation using the ultrafiltration protocol[14] (Figure S1B), which resulted in two fractions, fraction 1 (containing proteins and vesicles > 100 kDa) and fraction 2 (containing soluble proteins >10, < 100 kDa). Successful enrichment of exosomes in fraction 1 but not fraction 2 was verified by transmission electron microscopy (TEM) analysis (Figure S1C) and detection of the presence of Flotillin-1 (Figure S1D), a canonical exosome marker.[15,16] However, the amount of PTEN in fraction 1 was rather limited compared with fraction 2 (Figure S1D), indicating that exosome is not the main avenue of PTEN secretion.

We further excluded the possibility that PTEN was secreted via the conventional protein secretion pathway because treatment of brefeldin A (BFA), which blocks endoplasmic reticulum (ER) to Golgi trafficking of secreted proteins, showed no effect on the secretion of endogenous PTEN by 293T cells, although it almost completely inhibited the secretion of clusterin α chain, which is used as a positive control[17] (Figure S1E). This is in consistency with the fact that PTEN protein lacks a canonical secretion signal as predicted using SignalP (Figure S1F). To find clues of PTEN secretion pathway, we turned to PTEN-interacting proteins by focusing on proteins that had been reported to play a role in UPS pathways (Table S1). Interestingly, one of the PTEN-interacting proteins, heat shock protein 90 beta family member 1 (HSP90B1), has been reported to be one major player in the TMED10-channeled UPS (THU), a translocation pathway regulating vesicle entry and secretion of leaderless cargoes.[18] We confirmed the interaction of PTEN with HSP90B1, as well as TMED10 and heat shock protein 90 alpha family class B member 1 (HSP90AB1), the other two core components involved in THU (Figure 1C). TMED10 knockout by gRNAs or knockdown by short hairpin RNAs (shRNAs) significantly reduced, while overexpression of TMED10 further enhanced the amount of secreted PTEN (Figures 1D, 1E, and S1G). Also, depletion of either HSP90AB1 or HSP90B1 inhibited PTEN secretion, whereas their co-depletion showed the strongest effect (Figure 1F). These results suggest that THU might serve as a major avenue for PTEN secretion.

To consolidate the notion that PTEN is secreted via THU, we showed that PTEN co-localized with TMED10 on the ER-Golgi intermediate compartment (ERGIC) where TMED10 channel assembles[18] (Figure 1G), and that PTEN bound to similar regions in TMED10 as interleukin-1β (IL-1β), a typical THU-secreted protein[18] (Figure 1H). Considering that THU-secreted proteins contain a common recognition motif that directs their secretion by this pathway,[18] we uploaded the sequences of PTEN and IL-1β in the MEME-Suite website for the discovery of common motifs,[19] which returned three motifs as we named motifs 1–3 (Figure 1I). Deletion of motif 3 or mutation of five of the six amino acid residues in motif 3 significantly attenuated PTEN secretion by 293T cells (Figures 1J and S1H). More interestingly, the motif 3-homologous sequence in IL-1β was exactly the sequence that directs IL-1β secretion by THU.[18] Thus, we identified motif 3 as the common recognition motif of THU cargoes in PTEN.

By stepwise mutation of the five amino acid residues in motif 3, we identified tryptophan 274 (W274) to be the key amino acid residue that directs PTEN secretion by THU (Figures 1K and S1I), as summarized in Figure S1J. While PTEN directly interacts with TMED10 *in vitro*, mutation of W274 to a leucine (W274L) almost completely abolished this interaction (Figure 1L). In concert with this, tryptophan also serves as the key amino acid residue in the corresponding IL-1β motif.[18] Moreover, W274 of PTEN was highly conserved among species (Figure S1K). Taken together, TMED10 recognizes W274 of PTEN to direct its secretion by THU pathway.

Extracellular soluble PTEN inhibits tumor growth

To examine the existence of extracellular PTEN in the TME, tumor interstitial fluids (TIFs) from tumors generated by B16-F10 mouse melanoma cells subcutaneously grown in C57BL/6J mice were collected and subjected to ELISA for PTEN protein. The result showed that PTEN was present in the TIFs of B16-F10 tumors at a concentration of ~22 ng/mL. To determine the origin of PTEN in the TIFs, tumors were generated either by parental B16-F10 cells or a PTEN-knockout B16-F10 cell line (B16-F10-ΔPTEN). As a result, about 80% of PTEN was lost in the TIFs of B16-F10-ΔPTEN tumors compared with B16-F10 tumors (Figure 2A). By contrast, depletion of the four major types of immune cells by their antibodies, including macrophages, neutrophils, $CD8^+$ T, and natural killer (NK) cells, showed a much

(J and K) WB analysis of secreted PTEN in 293T-ΔPTEN cells transfected with the indicated plasmids.
(L) Anti-FLAG pull-down of TMED10 by the indicated PTEN derivatives.
Data are means ± SEM. Statistical significance was determined by two-tailed unpaired t test (B).
See also Figure S1 and Table S1.

Please cite this article in press as: Zhang et al., Secreted PTEN binds PLXDC2 on macrophages to drive antitumor immunity and tumor suppression, Developmental Cell (2024), https://doi.org/10.1016/j.devcel.2024.08.003

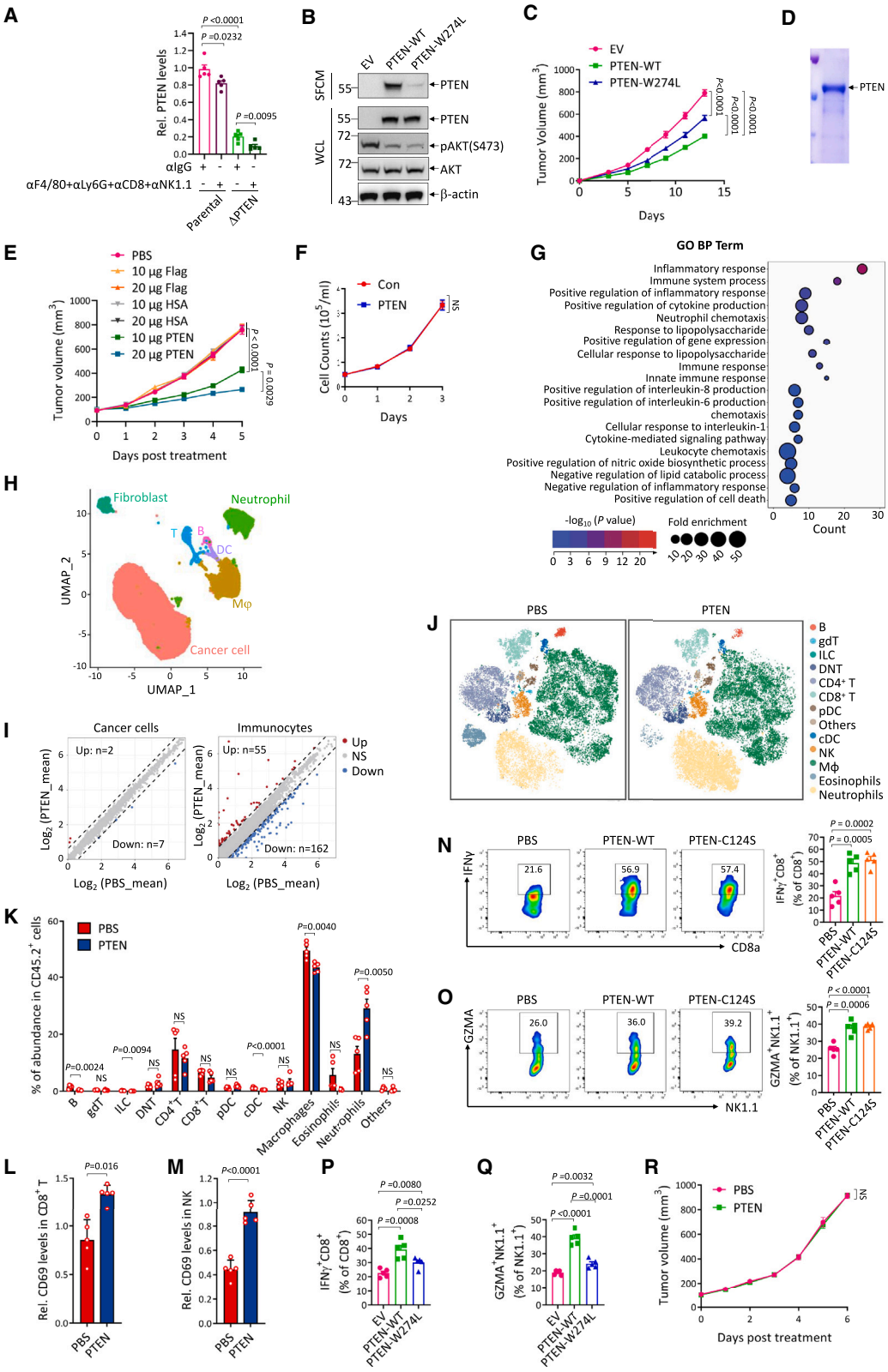

(legend on next page)

Please cite this article in press as: Zhang et al., Secreted PTEN binds PLXDC2 on macrophages to drive antitumor immunity and tumor suppression, Developmental Cell (2024), https://doi.org/10.1016/j.devcel.2024.08.003

weaker effect (Figure 2A). These results indicate that tumor cells serve as the major source of secreted PTEN in the TME.

To assess the role of secreted PTEN in the TME, PTEN-knockout MC38 cells (MC38-ΔPTEN) were subjected to re-expression of empty vector (EV), wild-type PTEN (PTEN-WT), or a PTEN mutant harboring W274L mutation (PTEN-W274L). PTEN-W274L was less efficiently secreted than PTEN-WT, whereas they inhibited AKT phosphorylation (Ser473) with similar strengths (Figure 2B), suggesting that W274L mutation selectively affects the secretion but not the phosphatase activity of PTEN. Then, these cell lines were subjected to subcutaneous growth in C57BL/6J mice, and the results revealed that PTEN-W274L had an impaired tumor-suppressing role compared with PTEN-WT (Figures 2C and S2A), suggesting that secreted PTEN might play a role in tumor suppression.

To further evaluate the role of secreted PTEN in tumor suppression, we sought to treat tumors directly with PTEN protein. PTEN protein was bacterially purified (Figure 2D) and injected into established tumors from B16-F10-ΔPTEN cells grown in C57BL/6J mice. The half-life of intratumorally injected PTEN was approximately 7 h (Figure S2B). For control treatment, PBS, human serum albumin (HSA), and FLAG peptide purified in parallel with PTEN protein were used. PTEN treatment manifested a significant tumor-suppressive effect in a dose-dependent manner compared with all control groups (Figures 2E and S2C). Because the three control treatments similarly behaved, only PBS was used hereafter. The tumor-suppressive effect of extracellular PTEN could also be recapitulated on tumors generated by MC38-ΔPTEN cells (Figures S2D and S2E). Of note, purified PTEN protein carrying a mutation that inactivates its phosphatase activity (PTEN-C124S) inhibited tumor growth to a similar level as PTEN-WT (Figures S2F and S2G). In addition, intraperitoneal injection of purified PTEN also significantly inhibited the growth of established B16-F10-ΔPTEN tumors (Figures S2H and S2I), with little effect on the body weight of mice (Figure S2J). Finally, we took advantage of the metastatic capacity of B16-F10 cells to examine the possible role of extracellular PTEN treatment on metastasis.[20] Micrometastases were seen in the lungs of B16-F10-ΔPTEN tumor-bearing mice as estimated by detecting the melanoma-specific *Trpm1* mRNA, which were significantly abolished by PTEN treatment (Figure S2K). Collectively, extracellular soluble PTEN exerts a tumor-suppressive role in a phosphatase activity-independent manner.

Extracellular PTEN elicits antitumor immune responses

In contrast to its tumor-suppressive effect *in vivo*, extracellular PTEN treatment did not affect the *in vitro* growth of B16-F10-ΔPTEN cells (Figure 2F), which hinted that it might act on the TME. Indeed, when PTEN-treated B16-F10-ΔPTEN tumors were analyzed by RNA sequencing (RNA-seq), Gene Ontology (GO) analysis of those 104 dysregulated genes revealed that they were mainly enriched in pathways involved in immune responses (Figures 2G and S2L). Especially, the strong activation of interferon α (IFNα) and IFNγ responses suggested that PTEN treatment elicits antitumor immune responses in the tumor (Figure S2M). Further, PTEN-treated and -untreated B16-F10-ΔPTEN tumors were subjected to single-cell RNA-seq (scRNA-seq), and major cell types were predicted using Seurat[21] (Figure 2H). The results showed that compared with cancer cells whose transcriptome was hardly disturbed, the transcriptome of immunocytes was substantially changed (Figure 2I), indicating that PTEN treatment preferentially altered the TIME.

To learn how PTEN affected the TIME, we used mass cytometry (CyTOF) to profile immune cells in PTEN-treated and -untreated B16-F10-ΔPTEN tumors (Figure 2J). The total number of neutrophils was most significantly changed, and that of macrophages was slightly altered, whereas those of $CD4^+$/$CD8^+$ T and NK cells were not affected (Figure 2K). However, in PTEN-treated tumors, the proportions of $CD8^+$ T and NK cells expressing the activation marker CD69 were significantly increased (Figures 2L and 2M). The enhanced activation of $CD8^+$ T and NK cells by PTEN-WT or PTEN-C124S treatment was further confirmed by flow cytometry analysis of IFNγ-positive $CD8^+$ T cells and granzyme A (GZMA)-positive NK cells in B16-F10-ΔPTEN tumors (Figures 2N and 2O), as well as in MC38-ΔPTEN tumors (Figures S2N and S2O). In concert with this, loss of PTEN secretion in MC38-ΔPTEN tumors contributes to an immunosuppressive phenotype (Figures 2P, 2Q, S2P, and S2Q). These

Figure 2. Extracellular PTEN elicits antitumor immune responses

(A) ELISA of PTEN in TIFs of the indicated B16-F10 tumors (n = 5).

(B and C) MC38-ΔPTEN cells transduced with EV, PTEN-WT, or PTEN-W274L were subjected to WB analysis of the indicated proteins (B) and subcutaneous growth in C57BL/6J mice (C, n = 5).

(D) Coomassie blue staining of bacterially purified PTEN.

(E) Subcutaneous growth of B16-F10-ΔPTEN tumors in C57BL/6J mice with the indicated treatments (n = 4).

(F) *In vitro* growth of B16-F10-ΔPTEN cells with or without PTEN treatment (n = 3).

(G) Gene Ontology (GO) analysis for differentially expressed genes in B16-F10-ΔPTEN tumors with or without PTEN treatment.

(H) Uniform manifold approximation and projection (UMAP) shows the results of single-cell dimensionality reduction and clustering. The colors of the labels correspond to the colors of the cell populations shown on the graph.

(I) Following the compartmentalization demonstrated in (H) into cancer cells and immunocytes (macrophages, neutrophils, DC, T, and B cells), scatterplots demonstrating the $\log_2$ average expression of genes in the PTEN treatment group and the control group were shown.

(J–M) t-distributed stochastic neighbor embedding (tSNE) plot of tumor-infiltrating leukocytes overlaid with color-coded clusters in B16-F10-ΔPTEN tumors with or without PTEN treatment (J), frequency of clusters of the indicated immune cell subsets (K), and relative CD69 expression on $CD8^+$ T (L) and NK cluster (M) were shown (n = 5).

(N and O) Percentages of IFNγ$^+$$CD8^+$ T cells (N) and GZMA$^+$NK1.1$^+$ NK cells (O) in B16-F10-ΔPTEN tumors with or without PTEN treatment (n = 5).

(P and Q) Percentages of IFNγ$^+$$CD8^+$ T cells (P) and GZMA$^+$NK1.1$^+$ NK cells (Q) in the indicated MC38-ΔPTEN tumors (n = 5).

(R) Subcutaneous growth of B16-F10-ΔPTEN tumors in NCG mice with or without PTEN treatment (n = 5).

Data are means ± SEM. Statistical significance was determined by two-tailed unpaired t test (A) and (K)–(Q) or two-way ANOVA (C), (E), (F), and (R). NS, non-significant.

See also Figure S2.

Please cite this article in press as: Zhang et al., Secreted PTEN binds PLXDC2 on macrophages to drive antitumor immunity and tumor suppression, Developmental Cell (2024), https://doi.org/10.1016/j.devcel.2024.08.003

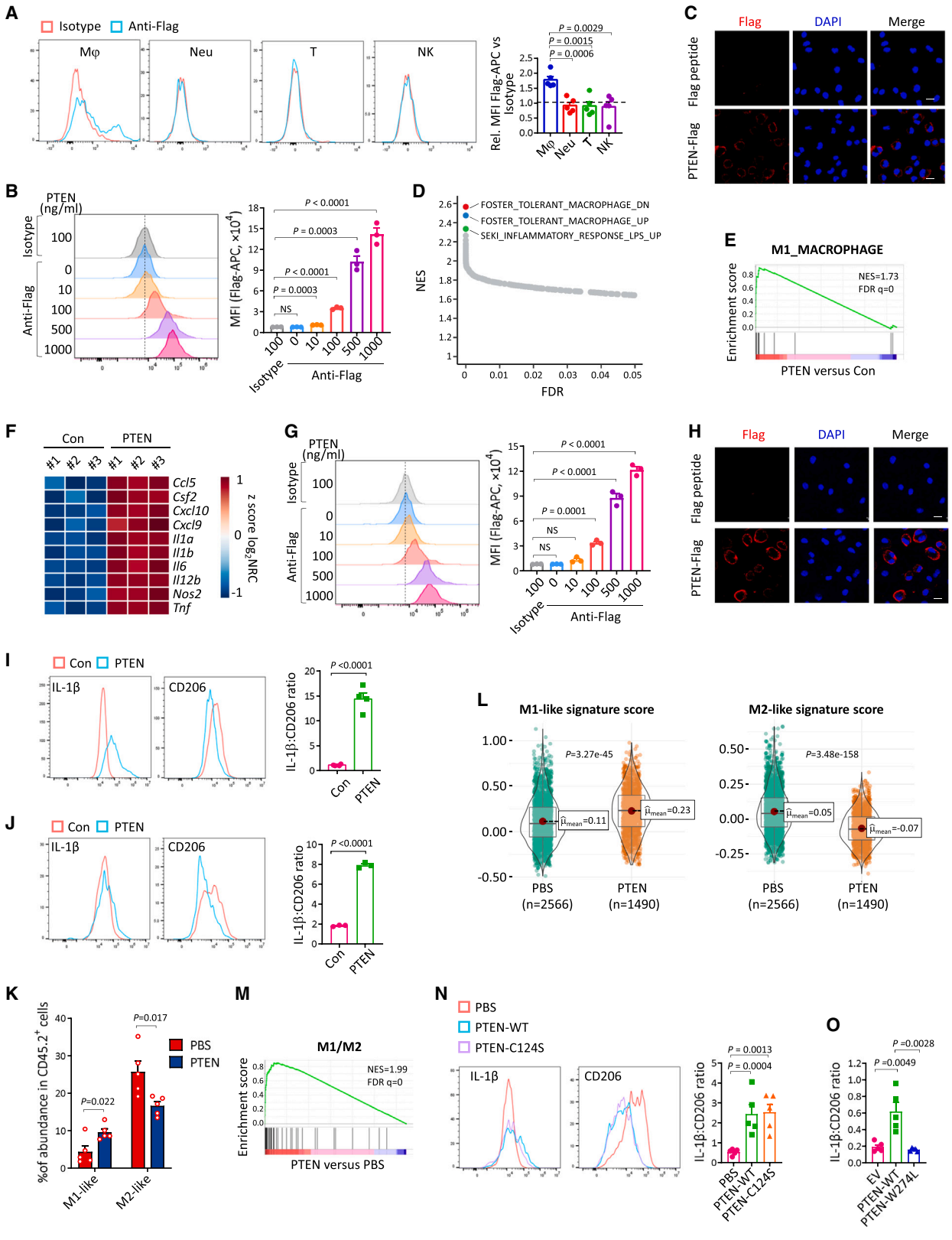

Figure 3. Extracellular PTEN binds to and polarizes macrophages toward an M1-like phenotype

(A) Binding of PTEN-FLAG to the surface of macrophages (Mφ), neutrophils (Neu), T, and NK cells isolated from B16-F10-ΔPTEN tumors (n = 5). MFI, mean fluorescence intensity. Dotted line indicates relative MFI = 1.

(legend continued on next page)

Please cite this article in press as: Zhang et al., Secreted PTEN binds PLXDC2 on macrophages to drive antitumor immunity and tumor suppression, Developmental Cell (2024), https://doi.org/10.1016/j.devcel.2024.08.003

results demonstrated that extracellular PTEN enhances antitumor immunity. Further, when B16-F10-ΔPTEN tumors grown in immunodeficient NCG mice were treated with PTEN,[22] no apparent effect on tumor growth was observed (Figures 2R and S2R), indicating that extracellular PTEN suppresses tumor growth in an immune response-dependent way.

Soluble PTEN binds to the surface of macrophages

Because PTEN was previously shown to be unable to enter cells without the assistance of delivery agents,[23] we speculated whether it binds to the surface of immune cells in the TME. We isolated the above-mentioned PTEN-regulated immune cells (macrophage, neutrophil, T, and NK) from PTEN-treated B16-F10-ΔPTEN tumors and tested the presence of PTEN on their surfaces. Among the four types of immune cells, only macrophages were labeled by PTEN (Figure 3A). The preference of PTEN in macrophage binding could be confirmed by incubating PTEN protein *in vitro* with immunes cells isolated from the spleens of C57BL/6J mice (Figure S3A). Also, PTEN binds to macrophages isolated from the bone marrow (bone marrow-derived macrophages, BMDMs) and abdominal cavity in a dose-dependent manner (Figures 3B and S3B). The presence of PTEN on the surface of BMDMs could also be visualized by performing immunofluorescent staining of PTEN after incubating FLAG-tagged PTEN with unpermeabilized BMDMs, whereas no intracellular signal was observed (Figure 3C). All these results demonstrated that PTEN binds to the surface of macrophages.

Extracellular PTEN polarizes macrophages toward an M1-like phenotype

To assess the consequence of PTEN binding on macrophages, we profiled the global transcriptome of PTEN-treated BMDMs. While PTEN treatment extensively altered the transcriptome of BMDMs (Figure S3C), gene set enrichment analysis (GSEA) revealed that the top three upregulated pathways were all related to lipopolysaccharide (LPS)-stimulated signaling[24,25] (Figure 3D). LPS is a conventional stimulator that induces proinflammatory (M1-like) polarization of BMDMs.[26,27] This promoted us to speculate whether PTEN induced naive BMDMs to undergo M1-like polarization. The notion was supported by GSEA using a signature depicting M1 polarization[28,29] (Figure 3E) and the dramatically increased expression of M1 markers in PTEN-treated BMDMs (Figure 3F). These results indicate that extracellular PTEN treatment polarizes naive BMDMs to M1-like phenotype.

Macrophages in TME are referred as tumor-associated macrophages (TAMs), which closely resemble the immunosuppressive M2-polarized macrophages.[30,31] To simulate the effect of PTEN on TAMs, naive BMDMs were treated with the cytokines IL-4 and IL-13 to induce M2-like polarization, before subjected to PTEN treatment. Binding of PTEN to the surface of unpermeabilized M2-polarized BMDMs could still be detected (Figures 3G and 3H). As a result, PTEN treatment increased the expression of M1 markers but decreased the expression of M2 markers (Figure S3D), and the expression ratio of IL-1β versus CD206 was significantly increased by PTEN treatment (Figure 3I). In addition, PTEN treatment also increased the expression ratio of IL-1β versus CD206 in TAMs generated by tumor-cell-conditioned medium (TCM) (Figure 3J). These results indicate that PTEN treatment converts M2-like macrophages toward M1-like phenotype *in vitro*.

To evaluate the effect of PTEN treatment on TAMs *in vivo*, we returned to our original CyTOF data, which showed that PTEN-treated tumors had significantly fewer M2-like but more M1-like macrophages (Figure 3K). We also calculated M1 and M2 gene signature-based scores at the single-cell level in TAMs using our scRNA-seq data. Overall, macrophages isolated from PTEN-treated B16-F10-ΔPTEN tumors showed significantly higher M1-gene signature scores but much lower M2-gene signature scores (Figure 3L). GSEA with a signature depicting M1/M2 conversion using our RNA-seq data supported that PTEN-treated tumors underwent M2 to M1 conversion[28,29] (Figure 3M). In addition, flow cytometry analysis showed that PTEN treatment increased the expression ratio of IL-1β versus CD206 of macrophages in B16-F10-ΔPTEN and MC38-ΔPTEN tumors (Figures 3N and S3E), and this role of PTEN was phosphatase-independent (Figure 3N). These data demonstrated that PTEN treatment skewed TAM polarization away from the M2-like phenotype toward M1-like phenotype. In concert with this, while re-expression of PTEN-WT in MC38-ΔPTEN tumors increased the expression ratio of IL-1β versus CD206 of macrophages, re-expression of PTEN-W274L showed a largely compromised effect (Figure 3O).

PTEN depends on macrophages to enhance antitumor immunity and suppress tumor growth

The above findings promoted us to ask whether extracellular PTEN depends on macrophages to enhance antitumor immunity and suppress tumor. We found that the tumor-suppressive effect of PTEN treatment was no longer observed in tumors depleted of

(B) Binding of PTEN-FLAG to BMDMs (n = 3).
(C) Confocal microscopy of PTEN-FLAG on BMDMs (scale bars, 10 μm).
(D and E) GSEA of RNA-seq data of BMDMs with or without PTEN treatment.
(F) Heatmap showing the indicated gene expression in BMDMs with or without PTEN treatment. NRC, normalized gene read counts.
(G) Binding of PTEN-FLAG to M2-polarized BMDMs (n = 3).
(H) Confocal microscopy of PTEN-FLAG on M2-polarized BMDMs (scale bars, 10 μm).
(I and J) IL-1β:CD206 MFI ratios of M2-polarized BMDMs (I, n = 4) and TCM-treated BMDMs (J, n = 3) with or without PTEN treatment.
(K) CyTOF analysis for the frequencies of the indicated macrophage subsets in B16-F10-ΔPTEN tumors with or without PTEN treatment (n = 5).
(L) Violin plot showing the expression-based score of M1-like and M2-like macrophage signatures, with their mean scores and p values labeled. Significance levels were computed using the Wilcoxon test.
(M) GSEA of RNA-seq data of B16-F10-ΔPTEN tumors with or without PTEN treatment with the indicated gene set.
(N and O) IL-1β:CD206 MFI ratios of TAMs in the indicated B16-F10-ΔPTEN (N) and MC38-ΔPTEN tumors (O) (n = 5).
Data are means ± SEM. Statistical significance was determined by two-tailed unpaired t test (A), (B), (G), (I)–(K), (N), and (O).
See also Figure S3.

Please cite this article in press as: Zhang et al., Secreted PTEN binds PLXDC2 on macrophages to drive antitumor immunity and tumor suppression, Developmental Cell (2024), https://doi.org/10.1016/j.devcel.2024.08.003

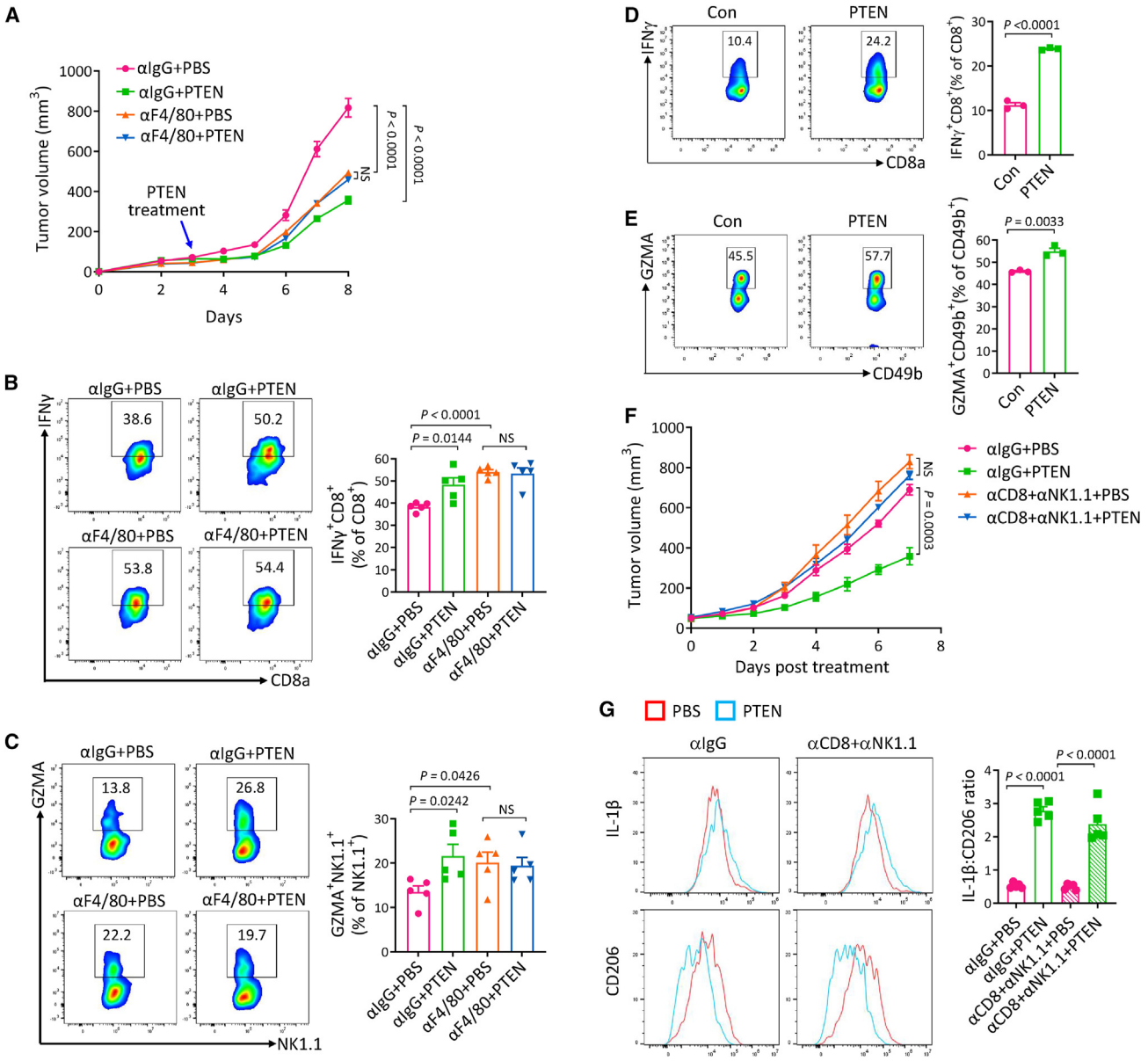

Figure 4. Extracellular PTEN depends on macrophages to enhance antitumor immunity and suppress tumor growth

(A–C) Subcutaneous growth (A) and percentages of IFNγ$^+$CD8$^+$ T cells (B) and GZMA$^+$NK1.1$^+$ NK cells (C) of B16-F10-ΔPTEN tumors subjected to the indicated treatments (n = 5).

(D and E) Percentages of IFNγ$^+$CD8$^+$ T cells (D) and GZMA$^+$CD49b$^+$ NK cells (E), respectively, in CD8$^+$ T cells and NK cells co-cultured with M2-polarized BMDMs pre-treated with or without PTEN (n = 3).

(F and G) Subcutaneous growth (F) and IL-1β:CD206 MFI ratios of TAMs (G) of B16-F10-ΔPTEN tumors subjected to the indicated treatments (n = 5).

Data are means ± SEM. Statistical significance was determined by two-way ANOVA (A) and (F) or two-tailed unpaired t test (B)–(E) and (G).

See also Figure S4.

macrophages by anti-F4/80 antibodies (Figures 4A and S4A), indicating that PTEN depends on the presence of macrophages to exert its tumor-suppressive role. Moreover, depletion of macrophages abolished the role of PTEN treatment in promoting the activation of CD8$^+$ T and NK cells (Figures 4B and 4C), suggesting that TAMs are required to mediate the activation of CD8$^+$ T and NK cells by PTEN treatment. This notion was further confirmed *in vitro*, as CD8$^+$ T and NK cells isolated from mice spleens were not activated by direct PTEN treatment (Figures S4B and S4C), but were activated by M2-polarized BMDMs pre-treated by PTEN (Figures 4D and 4E). On the other hand, co-depletion of CD8$^+$ T and NK cells with anti-CD8 and anti-NK1.1 antibodies almost completely abolished the tumor-suppressive effect of PTEN treatment (Figures 4F and S4D) but showed no effect on PTEN-induced M2 to M1 polarization of macrophages (Figure 4G). All these results demonstrated that

Please cite this article in press as: Zhang et al., Secreted PTEN binds PLXDC2 on macrophages to drive antitumor immunity and tumor suppression, Developmental Cell (2024), https://doi.org/10.1016/j.devcel.2024.08.003

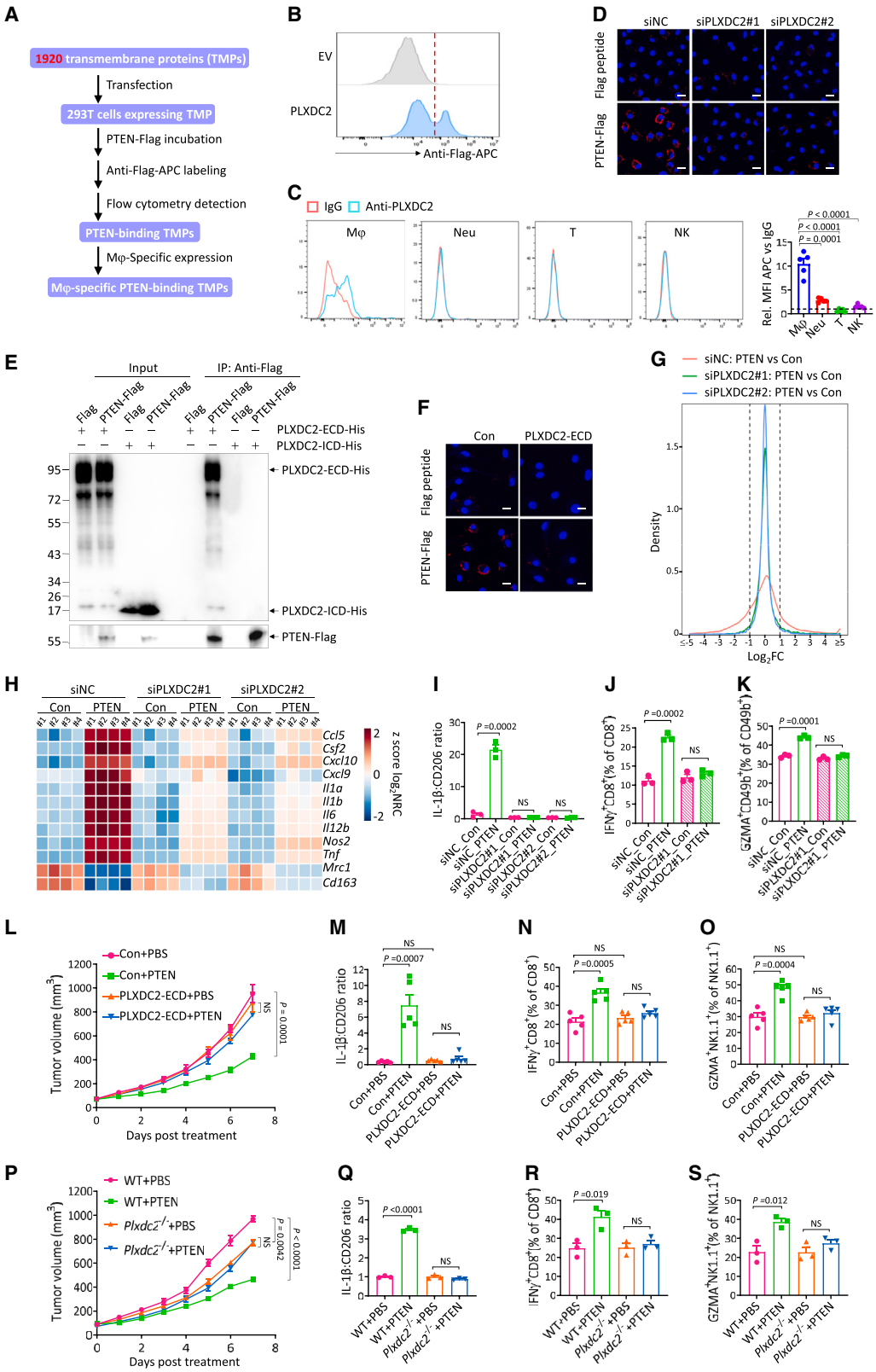

Figure 5. PTEN binds to PLXDC2 on macrophages to exert antitumor effects

(A) The workflow for identifying PTEN-binding transmembrane proteins (TMPs).

(B) Binding of PTEN-FLAG to 293T cells transfected with the indicated plasmids.

(legend continued on next page)

Please cite this article in press as: Zhang et al., Secreted PTEN binds PLXDC2 on macrophages to drive antitumor immunity and tumor suppression, Developmental Cell (2024), https://doi.org/10.1016/j.devcel.2024.08.003

polarization of macrophages is an upstream event of the activation of $CD8^+$ T and NK cells under PTEN treatment, and their sequential occurrences mediate the tumor-suppressive role of extracellular PTEN. Further, we revisited our scRNA-seq data to investigate interactions between macrophages and T cells based on ligand-receptor expression levels using the CellChat platform.[32] The result revealed that SPP1 (macrophages)-CD44 (T cells) axis, which plays an established role in mediating T cell suppression by TAMs,[33] was the most significantly affected cell-cell interaction between TAMs and T cells by PTEN treatment in B16-F10-ΔPTEN tumors (Figure S4E), further supporting that PTEN treatment alleviates T cell suppression by TAMs.

Because PTEN treatment significantly increased the total number of neutrophils, we also asked the role of increased neutrophils in extracellular PTEN-mediated tumor suppression. Although depletion of neutrophils with anti-Ly6G antibodies slightly slowed down tumor growth, PTEN treatment similarly inhibited the growth of neutrophil-depleted and non-depleted tumors (Figures S4F and S4G), indicating that the increased neutrophils are dispensable for extracellular PTEN-mediated tumor suppression in the current model. We also excluded the possibility that the increase of neutrophils is an upstream or downstream event of macrophage polarization as they were not affected by each other's depletion (Figures S4H and S4I). Therefore, the regulatory mechanism and role of increased neutrophils upon PTEN treatment warranted further investigation.

PTEN binds to PLXDC2 on macrophages to exert antitumor effects

Because PTEN did not enter but was preferentially bound to the surface of macrophages, we postulated that there was a macrophage-specific receptor for PTEN. To identify this receptor, we made use of a library of 1,920 transmembrane proteins (TMPs) (Table S2). A workflow illustrating the screening process is shown in Figure 5A. The screening generated one candidate, PLXDC2, which simultaneously fulfilled the criteria of mediating PTEN binding to 293T cells upon ectopic expression (Figure 5B) and presenting a macrophage-enriched expressional pattern in human cancer samples of various cancer types (Figure S5A). PLXDC2 is specifically expressed on the surface of macrophages but not neutrophils, T cells, or NK cells (Figure 5C), which mirrored the macrophage-specific binding of PTEN among these cells. PLXDC2 expression was detected on the surface of naive and M1- or M2-polarized BMDMs (Figure S5B), and its knockdown by two small interfering RNAs (siRNAs) largely prevented PTEN binding to M2-polarized BMDMs (Figures 5D and S5C). Finally, PTEN directly interacted with the extracellular domain (ECD) but not the intracellular domain (ICD) of PLXDC2 *in vitro* (Figure 5E) and did not interact with PLXDC2 lacking the ECD in the cells (Figure S5D). Addition of excessively purified PLXDC2-ECD into the culture medium abolished the binding of PTEN to the surface of M2-polarized BMDMs (Figure 5F). All these results supported that PLXDC2 is a PTEN receptor that mediates PTEN binding to the surface of macrophages.

To evaluate whether PLXDC2 mediated the role of PTEN on macrophages, we conducted RNA-seq on M2-polarized BMDMs with or without PLXDC2 knockdown in the presence or absence of PTEN treatment. In unsupervised principal-component analysis (PCA), knockdown of PLXDC2 significantly affected the transcriptome of M2-polarized BMDMs in the presence of PTEN treatment (Figure S5E). Further analysis revealed that each of the PLXDC2-targeting siRNAs reversed more than 95% of the gene alterations caused by PTEN treatment to a certain extent (Figures 5G and S5F), including those genes representing M2 to M1 transition (Figure 5H). The antagonizing effect of PLXDC2 knockdown on PTEN treatment-induced M1 polarization of naive and M2-polarized BMDMs was further confirmed by the expression ratio of IL-1β versus CD206 (Figures 5I, S5G, and S5H). These results indicate that PTEN depends on PLXDC2 to exert its role on macrophages. In accordance with this, PLXDC2-deficient BMDMs failed to mediate the role of extracellular PTEN in activating $CD8^+$ T and NK cells *in vitro* (Figures 5J, 5K, S5I, and S5J).

To determine the critical role of PLXDC2 in mediating the antitumor effects of PTEN *in vivo*, PTEN was administrated to B16-F10-ΔPTEN tumors alone or in combination with PLXDC2-ECD. The tumor-inhibitory effect of PTEN was almost completely abolished by the presence of PLXDC2-ECD (Figures 5L and S6A). Co-treatment of PLXDC2-ECD also blocked PTEN-induced M1 polarization of TAMs (Figures 5M and S6B) and activation of $CD8^+$ T and NK cells (Figures 5N, 5O, S6C, and S6D). These results indicate that binding to PLXDC2 is crucial for extracellular PTEN to elicit antitumor immunity and suppress tumor growth. To make sure that it was PLXDC2 on macrophages that mediated these effects of PTEN, we co-implanted WT or PLXDC2-knocked down BMDMs with B16-F10-ΔPTEN cells into recipient mice (Figure S6E) and found that the

(C) PLXDC2 expression on the indicated cells isolated from B16-F10-ΔPTEN tumors ($n = 5$). Dotted line indicates relative MFI = 1.
(D) Confocal microscopy of PTEN-FLAG on M2-polarized BMDMs with or without PLXDC2 knockdown (scale bars, 10 μm).
(E) Anti-FLAG pull-down of PLXDC2 derivatives by PTEN-FLAG.
(F) Confocal microscopy of PTEN-FLAG on M2-polarized BMDMs in the presence or absence of excessive PLXDC2-ECD (scale bars, 10 μm).
(G and H) M2-polarized BMDMs with or without PLXDC2 knockdown were treated with or without PTEN and subjected to RNA-seq analysis, with density plot demonstrating the gene expression alterations caused by PTEN treatment (G) and heatmap showing the indicated gene expression (H).
(I) IL-1β:CD206 MFI ratios of M2-polarized BMDMs subjected to the indicated treatments ($n = 3$).
(J and K) Percentages of $IFN\gamma^+CD8^+$ T cells (J) and $GZMA^+CD49b^+$ NK cells (K), respectively, in $CD8^+$ T cells and NK cells co-cultured with M2-polarized BMDMs subjected to the indicated treatments ($n = 3$).
(L–O) Subcutaneous growth (L), IL-1β:CD206 MFI ratios of TAMs (M), and percentages of $IFN\gamma^+CD8^+$ T cells (N) and $GZMA^+NK1.1^+$ NK cells (O) of B16-F10-ΔPTEN tumors subjected to the indicated treatments ($n = 5$).
(P–S) Subcutaneous growth (P, $n = 5$), IL-1β:CD206 MFI ratios of TAMs (Q, $n = 3$), and percentages of $IFN\gamma^+CD8^+$ T cells (R, $n = 3$) and $GZMA^+NK1.1^+$ NK cells (S, $n = 3$) of B16-F10-ΔPTEN tumors with or without PTEN treatment in WT and *Plxdc2*$^{-/-}$ mice.
Data are means ± SEM. Statistical significance was determined by two-tailed unpaired t test (C), (I)–(K), (M)–(O), and (Q)–(S) or two-way ANOVA (L) and (P).
See also Figures S5 and S6 and Table S2.

Please cite this article in press as: Zhang et al., Secreted PTEN binds PLXDC2 on macrophages to drive antitumor immunity and tumor suppression, Developmental Cell (2024), https://doi.org/10.1016/j.devcel.2024.08.003

CellPress

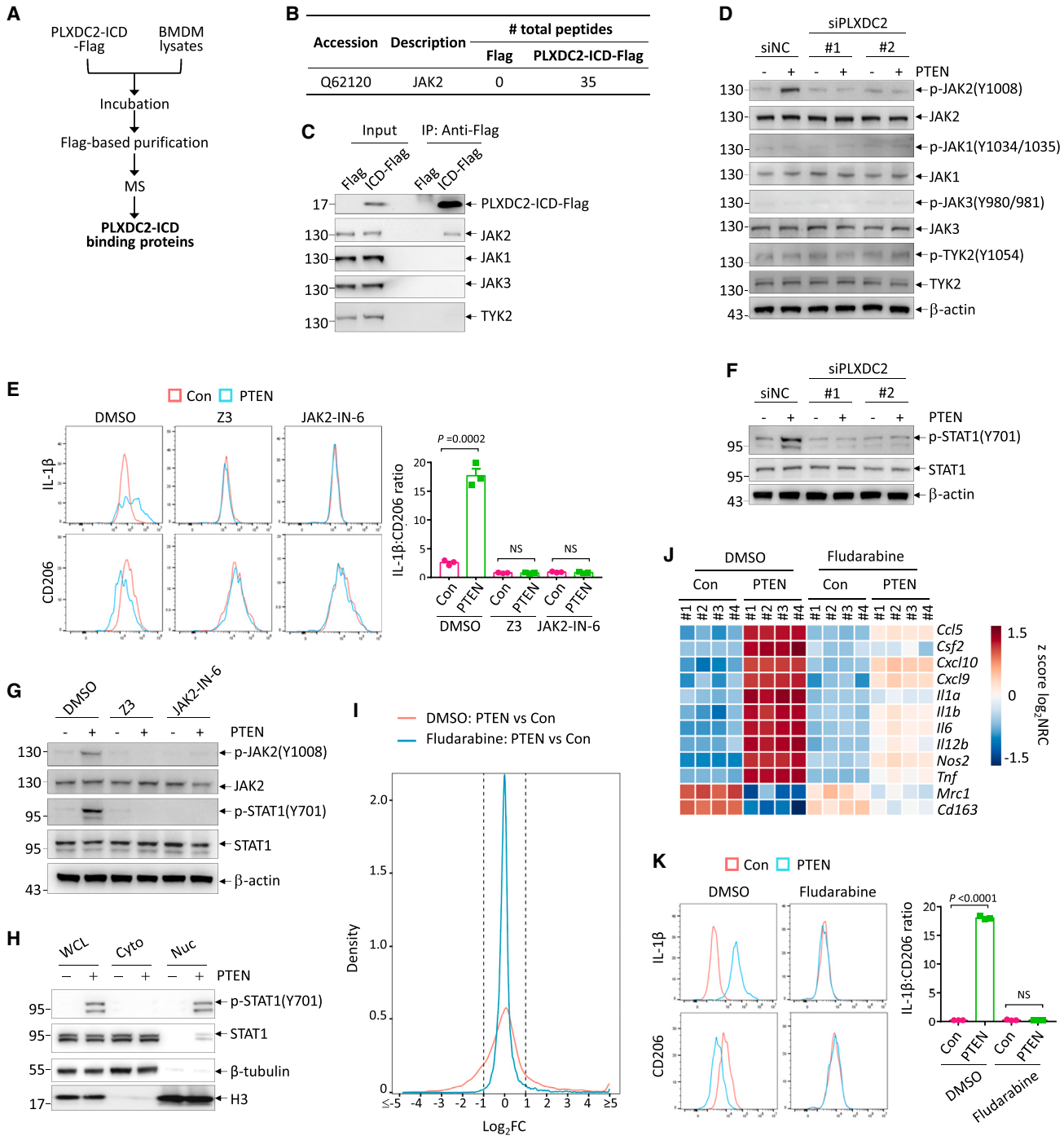

Figure 6. Engagement of PLXDC2 by PTEN activates JAK2-STAT1 signaling to reprogram macrophages

(A and B) The workflow for identifying proteins interacting with PLXDC2 intracellular domain (PLXDC2-ICD) in BMDMs (A). The mass spectrometry result of JAK2 is shown (B).

(C) BMDM lysates were incubated with FLAG or PLXDC2-ICD-FLAG and subjected to anti-FLAG coIP, followed by WB analysis of the indicated proteins.

(D) WB analysis for the indicated proteins in M2-polarized BMDMs subjected to the indicated treatments.

(E) IL-1β:CD206 MFI ratios of M2-polarized BMDMs subjected to the indicated treatments ($n = 3$).

(F and G) WB analysis for the indicated proteins in M2-polarized BMDMs subjected to the indicated treatments.

(H) WB analysis for the indicated proteins in WCL, cytoplasmic (Cyto), and nuclear (Nuc) fractions of M2-polarized BMDMs with or without PTEN treatment for 30 min.

(legend continued on next page)

Please cite this article in press as: Zhang et al., Secreted PTEN binds PLXDC2 on macrophages to drive antitumor immunity and tumor suppression, Developmental Cell (2024), https://doi.org/10.1016/j.devcel.2024.08.003

tumor-inhibitory effect of PTEN was hardly observed on tumors co-implanted with PLXDC2-knocked down macrophages (Figures S6F and S6G). Further, we obtained myeloid-specific *Plxdc2*-depleted (*Plxdc2*$^{-/-}$) mice and WT mice, in which B16-F10-ΔPTEN tumors were generated subcutaneously and treated with or without PTEN. While PTEN treatment showed significant inhibitory effect on tumors generated on WT mice, this effect was not observed on tumors generated in *Plxdc2*$^{-/-}$ mice (Figures 5P and S6H). In consistence, *Plxdc2*-depletion also resisted PTEN treatment-induced M2 to M1 polarization of macrophages (Figures 5Q and S6I) and the activation of CD8^{+} T and NK cells in B16-F10-ΔPTEN tumors (Figures 5R, 5S, S6J, and S6K). Together, these data demonstrated that extracellular PTEN relies on its interaction with PLXDC2 on the surface of macrophages to activate antitumor immunity and suppress tumor growth.

PTEN-PLXDC2 engagement activates JAK2-STAT1 signaling to reprogram macrophages

The downstream signaling of PLXDC2 is largely unknown. To find clues of PTEN-PLXDC2-initiated signaling in macrophages, we sought to identify proteins that bind to the ICD of PLXDC2 (Figure 6A). Among all the proteins identified to interact with PLXDC2-ICD (Table S3), Janus kinase 2 (JAK2) showed the strongest strength (Figure 6B). We verified the selective binding of PLXDC2-ICD to JAK2 but not other family members in BMDMs (Figure 6C) and the reciprocal interaction between full-length PLXDC2 and JAK2 ectopically expressed in 293T cells (Figures S6L and S6M).

JAKs serve as the cytoplasmic signaling components of cytokine receptors and are activated through cytokine-mediated trans-phosphorylation.[34–36] PTEN treatment increased the phosphorylation of JAK2 (Tyr1008) but not other JAKs in M2-polarized BMDMs (Figure 6D), which was abolished by knockdown of PLXDC2, indicating that extracellular PTEN activates JAK2 in a PLXDC2-dependent manner. Inhibition of JAK2 kinase activity by specific inhibitors Z3 and JAK2-IN-6 antagonized the effect of PTEN in inducing M1 polarization of M2-polarized BMDMs (Figure 6E). All these data demonstrated that engagement of PLXDC2 by PTEN activates JAK2 to modulate polarization of macrophages.

JAKs recruit and phosphorylate STAT proteins for further signal transduction.[34,37] Phosphorylation of STAT1 (Tyr701) but not other STATs was specifically increased by PTEN treatment in a PLXDC2- and JAK2-dependent manner (Figures 6F, 6G, and S6N), which resulted in nuclear accumulation of STAT1 protein (Figure 6H), indicating STAT1 activation by the PTEN-PLXDC2-JAK2 axis. STAT1 plays an established role in M1 polarization of macrophages.[38–41] Indeed, inhibition of STAT1 by its inhibitor fludarabine manifested a similar effect as knockdown of PLXDC2 in antagonizing the effects of extracellular PTEN on macrophage reprogramming (Figures 6I–6K and S6O). Collectively, we identify JAK2-STAT1 signaling to be responsible for mediating the downstream signaling of PTEN-PLXDC2 in macrophages.

Extracellular PTEN synergizes with PD-1 blockade to suppress tumor growth

M2-like TAMs have been shown to render treatment resistance to various therapeutic agents, including immunotherapy like PD-1 blockade.[11,42–44] We thus tested whether PTEN-induced reprogramming of pro-tumorigenic M2-like TAMs to an anti-tumor M1-like phenotype resulted in a consequent enhancement of response to immune checkpoint blockade. Monotherapy with either PTEN or PD-1-blocking antibodies reduced the size of B16-F10-ΔPTEN tumors, and combined PTEN/anti-PD-1 treatment showed the most significant effect (Figures 7A and S7A). Of note, PD-1 blockade did not affect the levels of extracellular PTEN in TIFs, lymphoid nodes, or blood (Figure S7B) or the expression levels of PLXDC2 on TAMs of B16-F10 tumor-bearing mice (Figure S7C), suggesting that PD-1 blockade works independently of the PTEN-PLXDC2 axis. CT26 colorectal and Lewis lung carcinoma (LLC) models are characterized with relative anti-PD-1 resistance.[45–47] As expected, PD-1 blockade showed no effect on the burden of CT26-ΔPTEN or LLC tumors, while PTEN treatment showed moderate antitumor effect (Figures 7B, 7C, S7D, and S7E). Combined PTEN/anti-PD-1 treatment led to significantly reduced tumor size in both models (Figures 7B, 7C, S7D, and S7E). Overall, PTEN treatment enhanced the therapeutic efficacy of anti-PD-1 treatment *in vivo*.

Patient-derived primary TAMs respond to PTEN treatment *ex vivo*

To evaluate the clinical implications of PLXDC2 on TAMs, we referred to a previously reported strategy.[48] Briefly, two gene signatures, respectively, representing PLXDC2^{+} and PLXDC2^{-} TAMs were created by re-analyzing three previously reported scRNA-seq datasets of CD45^{+} immune cells[49–51] (Figure S7F) and applied to the bulk RNA-seq dataset generated from the tumor tissues of melanoma patients (SKCM) from The Cancer Genome Atlas (TCGA) database by the deconvolution tool CIBERSORTx to obtain the proportions of PLXDC2^{+} and PLXDC2^{-} TAMs in each sample.[52] We then compared the survival of patients with low and high proportions of PLXDC2^{+} TAMs and found that patients with higher portion of PLXDC2^{+} TAMs showed poorer overall survival than those with lower portion of PLXDC2^{+} TAMs (Figure S7G). Similar results were obtained in patients of colon adenocarcinoma (COAD), esophageal carcinoma (ESCA), and liver hepatocellular carcinoma (LIHC) from TCGA database (Figure S7G). These data are consistence with our results showing delayed tumor growth in myeloid-specific *Plxdc2*-depleted mice (Figures 5P and S6H).

We then determined whether PTEN treatment could reprogram patient-derived primary TAMs *ex vivo*. Tumor-infiltrating TAMs were isolated from tumor tissues from patients with colorectal cancer and confirmed for the expression of PLXDC2

(I and J) RNA-seq analysis of M2-polarized BMDMs treated with fludarabine and PTEN alone or in combination, with density plot demonstrating the gene expression alterations caused by PTEN treatment (I) and heatmap showing the indicated gene expression (J).
(K) IL-1β:CD206 MFI ratios of M2-polarized BMDMs subjected to the indicated treatments (n = 3).
Data are means ± SEM. Statistical significance was determined by two-tailed unpaired t test (E) and (K).
See also Figure S6 and Table S3.

Please cite this article in press as: Zhang et al., Secreted PTEN binds PLXDC2 on macrophages to drive antitumor immunity and tumor suppression, Developmental Cell (2024), https://doi.org/10.1016/j.devcel.2024.08.003

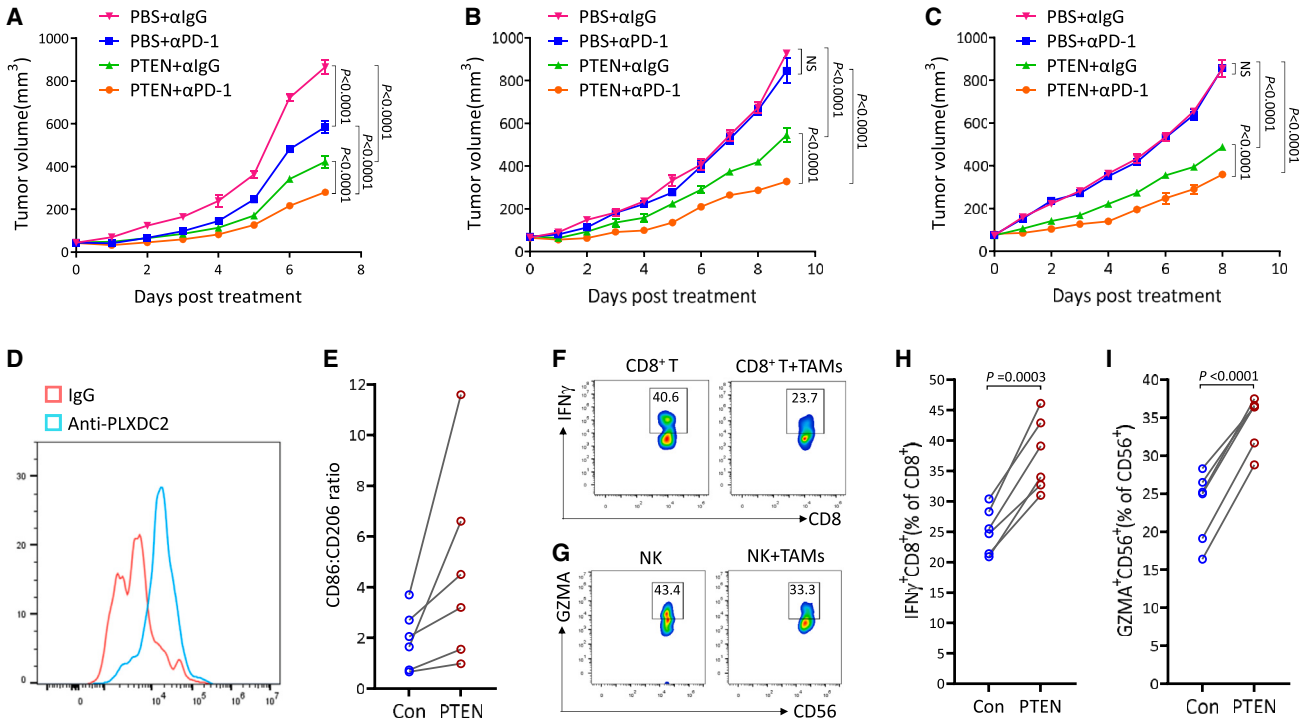

Figure 7. PTEN treatment synergizes with PD-1 blockade to suppress tumor growth and reprograms patient-derived primary TAMs *ex vivo*

(A–C) Subcutaneous growth of B16-F10-ΔPTEN (A), CT26-ΔPTEN (B), and LLC (C) tumors subjected to the indicated treatments (n = 5).

(D) PLXDC2 expression on TAMs isolated from one patient with colorectal cancer (CRC).

(E) CD86:CD206 MFI ratios of PTEN-treated and -untreated TAMs isolated from patients with CRC.

(F and G) Percentages of IFNγ$^+$CD8$^+$ T cells (F) and GZMA$^+$CD56$^+$ NK cells (G), respectively, in CD8$^+$ T cells and NK cells co-cultured with or without TAMs obtained from the same patient.

(H and I) Percentages of IFNγ$^+$CD8$^+$ T cells (H) and GZMA$^+$CD56$^+$ NK cells (I), respectively, in CD8$^+$ T cells and NK cells co-cultured with autogeneic TAMs pre-treated with or without PTEN (n = 6).

Data are means ± SEM. Statistical significance was determined by two-way ANOVA (A)–(C) and two-tailed paired t test (H) and (I).

See also Figure S7.

(Figure 7D). We found that TAMs from all patients showed increased expression ratio of CD86 versus CD206 upon PTEN treatment (Figure 7E), indicating that PTEN induces M2 to M1 polarization of patient-derived TAMs. We also isolated CD8$^+$ T and NK cells from the peripheral blood of each patient and exemplarily confirmed their suppression by autogeneic TAMs using samples from one patient (Figures 7F and 7G). Then, TAMs from each patient were treated with or without PTEN and subjected to incubation with autogeneic CD8$^+$ T and NK cells. The results showed that CD8$^+$ T and NK cells incubated with PTEN-treated TAMs showed a higher activity than those cultured with PTEN-untreated TAMs (Figures 7H, 7I, S7H, and S7I), supporting a role for PTEN in alleviating the immune-suppressive role of patient-derived TAMs. Thus, our *ex vivo* data demonstrated that TAMs from patient biopsies are responsive to PTEN treatment.

DISCUSSION

The finding that PTEN acts as a cytokine to regulate tumor immunity is unexpected. Although a relatively small portion of PTEN is secreted via exosome, PTEN-containing exosomes have been reported to transfer PTEN into other cells to compensate for PTEN loss in PTEN-deficient cells.[53] PTENα (also called PTEN-long[54]), a translational variant of PTEN, has been reported to be secreted by cells via secretion signals located within its N-terminal extensions (NTEs), and full-length PTENα has been reported to enter other cells via a cell-penetrating element located within its NTE to antagonize PI3K signaling and induce tumor cell death.[55,56] Therefore, while these sources of secreted PTEN serve the purpose to be taken up by and mediate non-cell-autonomous functions in recipient cells, our study identifies PTEN to be mainly secreted as a soluble protein that is not taken up by other cells but is recognized as a ligand by the receptor PLXDC2 expressed on the surface of macrophages to activate intracellular signaling.

Because PTEN is secreted by various cell lines, we expected that most cell types in the TME to secrete PTEN. However, our results indicate that tumor cells are the primary source of extracellular PTEN in the TME and that the status of PTEN in tumor cells decides the abundance of extracellular PTEN in the TME. One explanation for this is that tumor cells are numerically dominant in the tumor, as revealed by our scRNA-seq analysis of B16-F10 tumors (Figure 2H). Because PTEN undergoes frequent loss in most cancers due to genetic alterations or transcriptional/post-transcriptional inhibition, we would expect loss

Please cite this article in press as: Zhang et al., Secreted PTEN binds PLXDC2 on macrophages to drive antitumor immunity and tumor suppression, Developmental Cell (2024), https://doi.org/10.1016/j.devcel.2024.08.003

of extracellular PTEN is also common in cancer. This probably explains why immunosuppression is so prevalent in PTEN-dysregulated tumors, even though the mutation of the PTEN W274 residue does not exhibit a high frequency of reports in the COSMIC database.[57]

The TMP library we used to screen PTEN receptors in this study covers only a part of all TMPs. Therefore, it is possible that PTEN also binds to other TMPs besides PLXDC2, which may be localized on the surface of cells beyond macrophages. On the other hand, although PLXDC2 shows macrophage-specific expression, the cell types we covered in our analysis are limited, meaning that PLXDC2 might be expressed by other cells not tested in this study. For example, single-cell study identified PLXDC2 to be enriched not only in monocytes/macrophages but also in fibroblasts,[58] and proteomic analysis revealed PLXDC2 on the cell surface of human pluripotent stem cells.[59] PLXDC2, together with its homolog PLXDC1, was also identified to be the transmembrane receptor for pigment epithelium-derived factor (PEDF) in endothelial cells.[60] In view of these, we do not exclude the possibility that extracellular PTEN binds to the surface of cells beyond macrophages through PLXDC2 or potential unidentified receptors. This means that besides its role in reprogramming macrophages, extracellular PTEN may well-possess other functions. In support of this notion, treatment with extracellular PTEN significantly increased the number of neutrophils in the tumor without binding to neutrophils. Because this increase was independent of macrophages, this probably means that extracellular PTEN regulates neutrophils through binding to cells other than macrophages. The increased neutrophils are dispensable for the tumor-suppressive role of extracellular PTEN, although both anti-cancer and metastasis-facilitating functions of neutrophils have been reported.[61–64]

Although PLXDC2 is required to mediate the tumor-suppressive role of PTEN, its expression on TAMs in PTEN-untreated tumors seems to favor tumorigenesis, as revealed by the delayed tumor growth in myeloid-specific *Plxdc2*-depleted mice and the inverse correlation between PLXDC2 on TAMs and patient survival. Because of the frequent loss of PTEN in cancers, we reasoned that PLXDC2 on TAMs might normally be occupied by other ligands or simply unoccupied in the scarcity of PTEN, under which conditions PLXDC2 plays a tumor-promoting role, whereas the existence of PTEN in the TME re-occupies PLXDC2 with PTEN to activate the tumor-suppressive JAK2-STAT1 signaling.

Tumorigenesis is a genetic/epigenetic process driven by oncogene activation and tumor suppressor gene (TSG) inactivation.[65] However, it has been a major challenge to use standard pharmacologic approaches to target loss-of-function mutations of TSGs. In recent years, several promising strategies for targeting TSGs therapeutically have emerged, including synthetic lethality and collateral vulnerability screens, which aim to shut down signaling pathways that have been abnormally activated by loss of the TSG. However, so far, these efforts do not work well with PTEN.[6] Our discovery provides a clear rationale that the immunosuppressive phenotype caused by PTEN loss can be reversed by directly administrating PTEN protein in the tumor. Moreover, because PTEN administration works well on either PTEN-deficient or PTEN-intact tumors, this cytokine-like role of PTEN can probably be adopted to treat tumors even without PTEN loss.

Limitations of the study

The crystal structural basis of PTEN-PLXDC2 complex remains to be illustrated to provide theoretical basis for maximizing the therapeutic efficacy of PTEN. While the role of secreted PTEN is mainly investigated in the context of cancer here, its physiological relevance and pathological roles in other diseases remain to be explored. Lastly, the clinical relevance of PTEN immunogenicity and its impact on TME modulation deserve attention. Addressing whether PTEN mutations affect protein folding, leading to the production of anti-PTEN antibodies, and elucidating their role in PTEN blockade under physiological conditions would deepen our understanding of tumor immune evasion mechanisms.

STAR★METHODS

Detailed methods are provided in the online version of this paper and include the following:

- KEY RESOURCES TABLE
- RESOURCE AVAILABILITY
  - Lead contact
  - Materials availability
  - Data and code availability
- EXPERIMENTAL MODEL AND STUDY PARTICIPANT DETAILS
  - Cell lines
  - Mice
  - Human samples
- METHOD DETAILS
  - Western blot (WB)
  - Plasmids, shRNA, sgRNA and lentiviruses
  - Secretion determination
  - Immunoprecipitation (IP) and pull-down
  - Duolink PLA
  - Protein expression and purification
  - CRISPR-mediated knockout
  - Tumor treatment experiments
  - Cell isolation
  - Flow cytometry staining and analysis
  - Bone marrow-derived macrophages (BMDMs) polarization and stimulation
  - RNA sequencing (RNA-seq) and analysis
  - Single-cell RNA sequencing (scRNA-seq) and analysis
  - Cell interaction analysis
  - GO Term and Gene Set Enrichment Analysis (GSEA)
  - RT-qPCR
  - Enzyme-linked immunosorbent assay (ELISA)
  - Mass cytometry (CyTOF) and data analysis
  - siRNA knockdown studies
  - Purification of tumor-associated macrophages (TAMs) from human tumor samples
  - Macrophage depletion
  - Neutrophil depletion
  - $CD8^+$ T cell depletion
  - NK cell depletion
  - Immunofluorescence (IF)
  - In vitro co-culture with $CD8^+$ T cells or NK cells
- QUANTIFICATION AND STATISTICAL ANALYSIS

SUPPLEMENTAL INFORMATION

Supplemental information can be found online at https://doi.org/10.1016/j.devcel.2024.08.003.

ACKNOWLEDGMENTS

This work was supported by the National Key R&D Program of China (2020YFA0803403), the National Natural Science Foundation of China (82302931, 82202921, 82103233, and 92253303), CAMS Innovation Fund for Medical Sciences (CIFMS) (2019-I2M-5-051), Shanghai Scientific and Technological Innovation Action Plan (20JC1410100), Innovative research team of high-level local universities in Shanghai (SHSMU-ZDCX20211800), Shanghai Frontiers Science Center of Cellular Homeostasis and Human Diseases, the National Postdoctoral Program for Innovative Talents (BX20230231), China Postdoctoral Science Foundation (2023M732278), and Opening Foundation of State Key Laboratory of Systems Medicine for Cancer (KF2124-93).

AUTHOR CONTRIBUTIONS

C.Z., H.-M.M., and J.-M.S. performed most experiments. S.W. performed bioinformatic analysis. N.Z., Y.-L.X., C.-X.L., P.H., M.-K.G., X.-L.C., and Y.-X.Z. conducted partial experiments. J.-K.Z. helped to analyze and interpret data. G.-Q.C. and S.-M.S. designed and supervised the entire project and prepared the manuscript.

DECLARATION OF INTERESTS

The authors declare no competing interests.

Received: January 27, 2024
Revised: June 24, 2024
Accepted: August 5, 2024
Published: August 27, 2024

REFERENCES

1. Maehama, T., and Dixon, J.E. (1998). The tumor suppressor, PTEN/MMAC1, dephosphorylates the lipid second messenger, phosphatidylinositol 3,4,5-trisphosphate. J. Biol. Chem. *273*, 13375–13378. https://doi.org/10.1074/jbc.273.22.13375.
2. Lee, Y.R., Chen, M., and Pandolfi, P.P. (2018). The functions and regulation of the PTEN tumour suppressor: new modes and prospects. Nat. Rev. Mol. Cell Biol. *19*, 547–562. https://doi.org/10.1038/s41580-018-0015-0.
3. Milella, M., Falcone, I., Conciatori, F., Cesta Incani, U., Del Curatolo, A., Inzerilli, N., Nuzzo, C.M.A., Vaccaro, V., Vari, S., Cognetti, F., and Ciuffreda, L. (2015). PTEN: Multiple Functions in Human Malignant Tumors. Front. Oncol. *5*, 24. https://doi.org/10.3389/fonc.2015.00024.
4. Bazzichetto, C., Conciatori, F., Pallocca, M., Falcone, I., Fanciulli, M., Cognetti, F., Milella, M., and Ciuffreda, L. (2019). PTEN as a Prognostic/Predictive Biomarker in Cancer: An Unfulfilled Promise? Cancers (Basel) *11*, 435. https://doi.org/10.3390/cancers11040435.
5. Song, M.S., Salmena, L., and Pandolfi, P.P. (2012). The functions and regulation of the PTEN tumour suppressor. Nat. Rev. Mol. Cell Biol. *13*, 283–296. https://doi.org/10.1038/nrm3330.
6. McLoughlin, N.M., Mueller, C., and Grossmann, T.N. (2018). The Therapeutic Potential of PTEN Modulation: Targeting Strategies from Gene to Protein. Cell Chem. Biol. *25*, 19–29. https://doi.org/10.1016/j.chembiol.2017.10.009.
7. Vidotto, T., Melo, C.M., Castelli, E., Koti, M., Dos Reis, R.B., and Squire, J.A. (2020). Emerging role of PTEN loss in evasion of the immune response to tumours. Br. J. Cancer *122*, 1732–1743. https://doi.org/10.1038/s41416-020-0834-6.
8. Peng, W., Chen, J.Q., Liu, C., Malu, S., Creasy, C., Tetzlaff, M.T., Xu, C., McKenzie, J.A., Zhang, C., Liang, X., et al. (2016). Loss of PTEN Promotes Resistance to T Cell-Mediated Immunotherapy. Cancer Discov. *6*, 202–216. https://doi.org/10.1158/2159-8290.CD-15-0283.
9. George, S., Miao, D., Demetri, G.D., Adeegbe, D., Rodig, S.J., Shukla, S., Lipschitz, M., Amin-Mansour, A., Raut, C.P., Carter, S.L., et al. (2017). Loss of PTEN Is Associated with Resistance to Anti-PD-1 Checkpoint Blockade Therapy in Metastatic Uterine Leiomyosarcoma. Immunity *46*, 197–204. https://doi.org/10.1016/j.immuni.2017.02.001.
10. Toso, A., Revandkar, A., Di Mitri, D., Guccini, I., Proietti, M., Sarti, M., Pinton, S., Zhang, J., Kalathur, M., Civenni, G., et al. (2014). Enhancing chemotherapy efficacy in Pten-deficient prostate tumors by activating the senescence-associated antitumor immunity. Cell Rep. *9*, 75–89. https://doi.org/10.1016/j.celrep.2014.08.044.
11. Bergholz, J.S., Wang, Q., Wang, Q., Ramseier, M., Prakadan, S., Wang, W., Fang, R., Kabraji, S., Zhou, Q., Gray, G.K., et al. (2023). PI3Kβ controls immune evasion in PTEN-deficient breast tumours. Nature *617*, 139–146. https://doi.org/10.1038/s41586-023-05940-w.
12. Parsa, A.T., Waldron, J.S., Panner, A., Crane, C.A., Parney, I.F., Barry, J.J., Cachola, K.E., Murray, J.C., Tihan, T., Jensen, M.C., et al. (2007). Loss of tumor suppressor PTEN function increases B7-H1 expression and immunoresistance in glioma. Nat. Med. *13*, 84–88. https://doi.org/10.1038/nm1517.
13. Putz, U., Howitt, J., Doan, A., Goh, C.P., Low, L.H., Silke, J., and Tan, S.S. (2012). The Tumor Suppressor PTEN Is Exported in Exosomes and Has Phosphatase Activity in Recipient Cells. Sci. Signal. *5*, ra70. https://doi.org/10.1126/scisignal.2003084.
14. Lobb, R.J., Becker, M., Wen, S.W., Wong, C.S.F., Wiegmans, A.P., Leimgruber, A., and Möller, A. (2015). Optimized exosome isolation protocol for cell culture supernatant and human plasma. J. Extracell. Vesicles *4*, 27031. https://doi.org/10.3402/jev.v4.27031.
15. Mathivanan, S., Fahner, C.J., Reid, G.E., and Simpson, R.J. (2012). ExoCarta 2012: database of exosomal proteins, RNA and lipids. Nucleic Acids Res. *40*, D1241–D1244. https://doi.org/10.1093/nar/gkr828.
16. Simpson, R.J., Kalra, H., and Mathivanan, S. (2012). ExoCarta as a resource for exosomal research. J. Extracell. Vesicles *1*. https://doi.org/10.3402/jev.v1i0.18374.
17. O'Sullivan, J., Whyte, L., Drake, J., and Tenniswood, M. (2003). Alterations in the post-translational modification and intracellular trafficking of clusterin in MCF-7 cells during apoptosis. Cell Death Differ. *10*, 914–927. https://doi.org/10.1038/sj.cdd.4401254.
18. Zhang, M., Liu, L., Lin, X.B., Wang, Y., Li, Y., Guo, Q., Li, S.L., Sun, Y.X., Tao, X., Zhang, D., et al. (2020). A Translocation Pathway for Vesicle-Mediated Unconventional Protein Secretion. Cell *181*, 637–652.e15. https://doi.org/10.1016/j.cell.2020.03.031.
19. Bailey, T.L., and Elkan, C. (1994). Fitting a mixture model by expectation maximization to discover motifs in biopolymers. Proc. Int. Conf. Intell. Syst. Mol. Biol. *2*, 28–36.
20. Wang, G., Li, J., Bojmar, L., Chen, H., Li, Z., Tobias, G.C., Hu, M., Homan, E.A., Lucotti, S., Zhao, F., et al. (2023). Tumour extracellular vesicles and particles induce liver metabolic dysfunction. Nature *618*, 374–382. https://doi.org/10.1038/s41586-023-06114-4.
21. Stuart, T., Butler, A., Hoffman, P., Hafemeister, C., Papalexi, E., Mauck, W.M., 3rd, Hao, Y., Stoeckius, M., Smibert, P., and Satija, R. (2019). Comprehensive Integration of Single-Cell Data. Cell *177*, 1888–1902.e21. https://doi.org/10.1016/j.cell.2019.05.031.
22. Amendola, C.R., Mahaffey, J.P., Parker, S.J., Ahearn, I.M., Chen, W.C., Zhou, M., Court, H., Shi, J., Mendoza, S.L., Morten, M.J., et al. (2019). KRAS4A directly regulates hexokinase 1. Nature *576*, 482–486. https://doi.org/10.1038/s41586-019-1832-9.
23. Altınoğlu, S.A., Wang, M., Li, K.Q., Li, Y., and Xu, Q. (2016). Intracellular delivery of the PTEN protein using cationic lipidoids for cancer therapy. Biomater. Sci. *4*, 1773–1780. https://doi.org/10.1039/c6bm00580b.
24. Foster, S.L., Hargreaves, D.C., and Medzhitov, R. (2007). Gene-specific control of inflammation by TLR-induced chromatin modifications. Nature *447*, 972–978. https://doi.org/10.1038/nature05836.
25. Seki, E., De Minicis, S., Osterreicher, C.H., Kluwe, J., Osawa, Y., Brenner, D.A., and Schwabe, R.F. (2007). TLR4 enhances TGF-beta signaling and hepatic fibrosis. Nat. Med. *13*, 1324–1332. https://doi.org/10.1038/nm1663.

26. Qin, H., Holdbrooks, A.T., Liu, Y., Reynolds, S.L., Yanagisawa, L.L., and Benveniste, E.N. (2012). SOCS3 deficiency promotes M1 macrophage polarization and inflammation. J. Immunol. *189*, 3439–3448. https://doi.org/10.4049/jimmunol.1201168.

27. Liu, P.S., Chen, Y.T., Li, X., Hsueh, P.C., Tzeng, S.F., Chen, H., Shi, P.Z., Xie, X., Parik, S., Planque, M., et al. (2023). CD40 signal rewires fatty acid and glutamine metabolism for stimulating macrophage anti-tumorigenic functions. Nat. Immunol. *24*, 452–462. https://doi.org/10.1038/s41590-023-01430-3.

28. Ou, D.L., Chen, C.W., Hsu, C.L., Chung, C.H., Feng, Z.R., Lee, B.S., Cheng, A.L., Yang, M.H., and Hsu, C. (2021). Regorafenib enhances antitumor immunity via inhibition of p38 kinase/Creb1/Klf4 axis in tumor-associated macrophages. J. Immunother. Cancer *9*, e001657. https://doi.org/10.1136/jitc-2020-001657.

29. Jablonski, K.A., Amici, S.A., Webb, L.M., Ruiz-Rosado, D., Popovich, P.G., Partida-Sanchez, S., and Guerau-de-Arellano, M. (2015). Novel Markers to Delineate Murine M1 and M2 Macrophages. PLoS One *10*, e0145342. https://doi.org/10.1371/journal.pone.0145342.

30. Chanmee, T., Ontong, P., Konno, K., and Itano, N. (2014). Tumor-associated macrophages as major players in the tumor microenvironment. Cancers (Basel) *6*, 1670–1690. https://doi.org/10.3390/cancers6031670.

31. Sica, A., Schioppa, T., Mantovani, A., and Allavena, P. (2006). Tumour-associated macrophages are a distinct M2 polarised population promoting tumour progression: potential targets of anti-cancer therapy. Eur. J. Cancer *42*, 717–727. https://doi.org/10.1016/j.ejca.2006.01.003.

32. Jin, S., Guerrero-Juarez, C.F., Zhang, L., Chang, I., Ramos, R., Kuan, C.H., Myung, P., Plikus, M.V., and Nie, Q. (2021). Inference and analysis of cell-cell communication using CellChat. Nat. Commun. *12*, 1088. https://doi.org/10.1038/s41467-021-21246-9.

33. Klement, J.D., Paschall, A.V., Redd, P.S., Ibrahim, M.L., Lu, C., Yang, D., Celis, E., Abrams, S.I., Ozato, K., and Liu, K. (2018). An osteopontin/CD44 immune checkpoint controls CD8+ T cell activation and tumor immune evasion. J. Clin. Invest. *128*, 5549–5560. https://doi.org/10.1172/JCI123360.

34. O'Shea, J.J., Holland, S.M., and Staudt, L.M. (2013). JAKs and STATs in immunity, immunodeficiency, and cancer. N. Engl. J. Med. *368*, 161–170. https://doi.org/10.1056/NEJMra1202117.

35. Wang, X., Lupardus, P., Laporte, S.L., and Garcia, K.C. (2009). Structural biology of shared cytokine receptors. Annu. Rev. Immunol. *27*, 29–60. https://doi.org/10.1146/annurev.immunol.24.021605.090616.

36. Hubbard, S.R. (2017). Mechanistic Insights into Regulation of JAK2 Tyrosine Kinase. Front. Endocrinol. (Lausanne) *8*, 361. https://doi.org/10.3389/fendo.2017.00361.

37. Levy, D.E., and Darnell, J.E., Jr. (2002). Stats: transcriptional control and biological impact. Nat. Rev. Mol. Cell Biol. *3*, 651–662. https://doi.org/10.1038/nrm909.

38. Xia, T., Fu, S., Yang, R., Yang, K., Lei, W., Yang, Y., Zhang, Q., Zhao, Y., Yu, J., Yu, L., and Zhang, T. (2023). Advances in the study of macrophage polarization in inflammatory immune skin diseases. J. Inflamm. (Lond) *20*, 33. https://doi.org/10.1186/s12950-023-00360-z.

39. Sica, A., and Mantovani, A. (2012). Macrophage plasticity and polarization: in vivo veritas. J. Clin. Invest. *122*, 787–795. https://doi.org/10.1172/JCI59643.

40. Yoshimura, A. (2006). Signal transduction of inflammatory cytokines and tumor development. Cancer Sci. *97*, 439–447. https://doi.org/10.1111/j.1349-7006.2006.00197.x.

41. Sica, A., and Bronte, V. (2007). Altered macrophage differentiation and immune dysfunction in tumor development. J. Clin. Invest. *117*, 1155–1166. https://doi.org/10.1172/JCI31422.

42. Wang, Q., Bergholz, J.S., Ding, L., Lin, Z., Kabraji, S.K., Hughes, M.E., He, X., Xie, S., Jiang, T., Wang, W., et al. (2022). STING agonism reprograms tumor-associated macrophages and overcomes resistance to PARP inhibition in BRCA1-deficient models of breast cancer. Nat. Commun. *13*, 3022. https://doi.org/10.1038/s41467-022-30568-1.

43. Halbrook, C.J., Pontious, C., Kovalenko, I., Lapienyte, L., Dreyer, S., Lee, H.J., Thurston, G., Zhang, Y., Lazarus, J., Sajjakulnukit, P., et al. (2019). Macrophage-Released Pyrimidines Inhibit Gemcitabine Therapy in Pancreatic Cancer. Cell Metab. *29*, 1390–1399.e6. https://doi.org/10.1016/j.cmet.2019.02.001.

44. Olson, O.C., Kim, H., Quail, D.F., Foley, E.A., and Joyce, J.A. (2017). Tumor-Associated Macrophages Suppress the Cytotoxic Activity of Antimitotic Agents. Cell Rep. *19*, 101–113. https://doi.org/10.1016/j.celrep.2017.03.038.

45. Samstein, R.M., Krishna, C., Ma, X., Pei, X., Lee, K.W., Makarov, V., Kuo, F., Chung, J., Srivastava, R.M., Purohit, T.A., et al. (2021). Mutations in BRCA1 and BRCA2 differentially affect the tumor microenvironment and response to checkpoint blockade immunotherapy. Nat. Cancer *1*, 1188–1203. https://doi.org/10.1038/s43018-020-00139-8.

46. Li, S., Simoni, Y., Zhuang, S., Gabel, A., Ma, S., Chee, J., Islas, L., Cessna, A., Creaney, J., Bradley, R.K., et al. (2021). Characterization of neoantigen-specific T cells in cancer resistant to immune checkpoint therapies. Proc. Natl. Acad. Sci. USA *118*, e2025570118. https://doi.org/10.1073/pnas.2025570118.

47. Chen, H.M., van der Touw, W., Wang, Y.S., Kang, K., Mai, S., Zhang, J., Alsina-Beauchamp, D., Duty, J.A., Mungamuri, S.K., Zhang, B., et al. (2018). Blocking immunoinhibitory receptor LILRB2 reprograms tumor-associated myeloid cells and promotes antitumor immunity. J. Clin. Invest. *128*, 5647–5662. https://doi.org/10.1172/JCI97570.

48. Kim, J., Kim, T.J., Chae, S., Ha, H., Park, Y., Park, S., Yoon, C.J., Lim, S.A., Lee, H., Kim, J., et al. (2024). Targeted deletion of CD244 on monocytes promotes differentiation into anti-tumorigenic macrophages and potentiates PD-L1 blockade in melanoma. Mol. Cancer *23*, 45. https://doi.org/10.1186/s12943-024-01936-w.

49. Zhang, X., Peng, L., Luo, Y., Zhang, S., Pu, Y., Chen, Y., Guo, W., Yao, J., Shao, M., Fan, W.J.N.c., et al. (2021). Dissecting esophageal squamous-cell carcinoma ecosystem by single-cell transcriptomic analysis. Nat. Commun. *12*, 5291. https://doi.org/10.1038/s41467-021-25539-x.

50. Ma, L., Wang, L., Khatib, S.A., Chang, C.-W., Heinrich, S., Dominguez, D.A., Forgues, M., Candia, J., Hernandez, M.O., Kelly, M.J.J.o.h., et al. (2021). Single-cell atlas of tumor cell evolution in response to therapy in hepatocellular carcinoma and intrahepatic cholangiocarcinoma. J. Hepatol. *75*, 1397–1408. https://doi.org/10.1016/j.jhep.2021.06.028.

51. Pelka, K., Hofree, M., Chen, J.H., Sarkizova, S., Pirl, J.D., Jorgji, V., Bejnood, A., Dionne, D., William, H.G., Xu, K.H.J.C., et al. (2021). Spatially organized multicellular immune hubs in human colorectal cancer. Cell *184*, 4734–4752.e20. https://doi.org/10.1016/j.cell.2021.08.003.

52. Newman, A.M., Liu, C.L., Green, M.R., Gentles, A.J., Feng, W., Xu, Y., Hoang, C.D., Diehn, M., and Alizadeh, A.A. (2015). Robust enumeration of cell subsets from tissue expression profiles. Nat. Methods *12*, 453–457. https://doi.org/10.1038/nmeth.3337.

53. Gabriel, K., Ingram, A., Austin, R., Kapoor, A., Tang, D., Majeed, F., Qureshi, T., and Al-Nedawi, K. (2013). Regulation of the tumor suppressor PTEN through exosomes: a diagnostic potential for prostate cancer. PLoS One *8*, e70047. https://doi.org/10.1371/journal.pone.0070047.

54. Liang, H., He, S., Yang, J., Jia, X., Wang, P., Chen, X., Zhang, Z., Zou, X., McNutt, M.A., Shen, W.H., and Yin, Y. (2014). PTENα, a PTEN isoform translated through alternative initiation, regulates mitochondrial function and energy metabolism. Cell Metab. *19*, 836–848. https://doi.org/10.1016/j.cmet.2014.03.023.

55. Hopkins, B.D., Fine, B., Steinbach, N., Dendy, M., Rapp, Z., Shaw, J., Pappas, K., Yu, J.S., Hodakoski, C., Mense, S., et al. (2013). A secreted PTEN phosphatase that enters cells to alter signaling and survival. Science *341*, 399–402. https://doi.org/10.1126/science.1234907.

56. Zhang, C., Ma, H.M., Dong, S.S., Zhang, N., He, P., Ge, M.K., Xia, L., Yu, J.X., Xia, Q., Chen, G.Q., and Shen, S.M. (2022). Furin extracellularly cleaves secreted PTENα/β to generate C-terminal fragment with a tumor-suppressive role. Cell Death Dis. *13*, 532. https://doi.org/10.1038/s41419-022-04988-2.

57. Tate, J.G., Bamford, S., Jubb, H.C., Sondka, Z., Beare, D.M., Bindal, N., Boutselakis, H., Cole, C.G., Creatore, C., Dawson, E., et al. (2019). COSMIC: the Catalogue Of Somatic Mutations In Cancer. Nucleic Acids Res. *47*, D941–D947. https://doi.org/10.1093/nar/gky1015.

58. Guan, Y., Du, Y., Wang, G., Gou, H., Xue, Y., Xu, J., Li, E., Chan, D.W., Wu, D., Xu, P., et al. (2021). Overexpression of PLXDC2 in Stromal Cell-Associated M2 Macrophages Is Related to EMT and the Progression of Gastric Cancer. Front. Cell Dev. Biol. *9*, 673295. https://doi.org/10.3389/fcell.2021.673295.

59. Boheler, K.R., Bhattacharya, S., Kropp, E.M., Chuppa, S., Riordon, D.R., Bausch-Fluck, D., Burridge, P.W., Wu, J.C., Wersto, R.P., Chan, G.C., et al. (2014). A human pluripotent stem cell surface N-glycoproteome resource reveals markers, extracellular epitopes, and drug targets. Stem Cell Rep. *3*, 185–203. https://doi.org/10.1016/j.stemcr.2014.05.002.

60. Cheng, G., Zhong, M., Kawaguchi, R., Kassai, M., Al-Ubaidi, M., Deng, J., Ter-Stepanian, M., and Sun, H. (2014). Identification of PLXDC1 and PLXDC2 as the transmembrane receptors for the multifunctional factor PEDF. eLife *3*, e05401. https://doi.org/10.7554/eLife.05401.

61. Coffelt, S.B., Kersten, K., Doornebal, C.W., Weiden, J., Vrijland, K., Hau, C.S., Verstegen, N.J.M., Ciampricotti, M., Hawinkels, L.J.A.C., Jonkers, J., and de Visser, K.E. (2015). IL-17-producing γδ T cells and neutrophils conspire to promote breast cancer metastasis. Nature *522*, 345–348. https://doi.org/10.1038/nature14282.

62. Coffelt, S.B., Wellenstein, M.D., and de Visser, K.E. (2016). Neutrophils in cancer: neutral no more. Nat. Rev. Cancer *16*, 431–446. https://doi.org/10.1038/nrc.2016.52.

63. Yan, J., Kloecker, G., Fleming, C., Bousamra, M., 2nd, Hansen, R., Hu, X., Ding, C., Cai, Y., Xiang, D., Donninger, H., et al. (2014). Human polymorphonuclear neutrophils specifically recognize and kill cancerous cells. Oncoimmunology *3*, e950163. https://doi.org/10.4161/15384101.2014.950163.

64. Sagiv, J.Y., Michaeli, J., Assi, S., Mishalian, I., Kisos, H., Levy, L., Damti, P., Lumbroso, D., Polyansky, L., Sionov, R.V., et al. (2015). Phenotypic diversity and plasticity in circulating neutrophil subpopulations in cancer. Cell Rep. *10*, 562–573. https://doi.org/10.1016/j.celrep.2014.12.039.

65. Croce, C.M. (2008). Oncogenes and cancer. N. Engl. J. Med. *358*, 502–511. https://doi.org/10.1056/NEJMra072367.

Please cite this article in press as: Zhang et al., Secreted PTEN binds PLXDC2 on macrophages to drive antitumor immunity and tumor suppression, Developmental Cell (2024), https://doi.org/10.1016/j.devcel.2024.08.003

STAR★METHODS

KEY RESOURCES TABLE

REAGENT or RESOURCE	SOURCE	IDENTIFIER
Antibodies		
Anti-mouse CD16/32	Biolegend	Cat# 156603; RRID: AB_2783137
Anti-Flag tag APC	Biolegend	Cat# 637308; RRID: AB_2561497
Anti-mouse CD45.2 FITC	Biolegend	Cat# 109805; RRID: AB_313442
Anti-mouse CD8a APC	Biolegend	Cat# 100711; RRID: AB_312750
Anti-mouse CD206 (MMR) APC	Biolegend	Cat# 141708; RRID: AB_10896057
Anti-mouse CD3e PE	Biolegend	Cat# 100308; RRID: AB_312672
Anti-mouse CD49b APC	Biolegend	Cat# 108910; RRID: AB_313416
Anti-mouse CD49b PE	Biolegend	Cat# 108907; RRID: AB_313415
Anti-mouse F4/80 PE	Biolegend	Cat# 123110; RRID: AB_893498
Anti-mouse CD4 PE	Biolegend	Cat# 100511; RRID: AB_312714
Anti-mouse NK-1.1 PE/Cyanine7	Biolegend	Cat# 108713; RRID: AB_389363
Anti-mouse Ly6G PE/Cyanine7	Biolegend	Cat# 127617; RRID: AB_1877261
Anti-mouse IFNγ BV421	Biolegend	Cat# 505830; RRID: AB_2563105
Anti-mouse CD3e PE/Cyanine7	Biolegend	Cat# 100320; RRID: AB_312685
Anti-mouse/human CD45R/B220 FITC	Biolegend	Cat# 103205; RRID: AB_312990
Anti-mouse Granzyme A PE	eBioscience	Cat# 12-5831-82; RRID: AB_2572631
Anti-mouse IL-1β PE-Cyanine7	eBioscience	Cat# 25-7114-82; RRID: AB_2573526
Anti-human CD45 APC	Biolegend	Cat# 982304; RRID: AB_2650648
Anti-human CD11b PE	Biolegend	Cat# 301306; RRID: AB_2650648
Anti-human CD14 FITC	Biolegend	Cat# 301804; RRID: AB_314186
Anti-human CD206 (MMR) APC	Biolegend	Cat# 321109; RRID: AB_571884
Anti-human CD86 PE/Cyanine7	Biolegend	Cat# 374209; RRID: AB_2728391
Anti-human Granzyme A APC	Biolegend	Cat# 507219; RRID: AB_2721454
Anti-human CD56 (NCAM) PE	Biolegend	Cat# 362507; RRID: AB_2564161
Anti-human CD8 APC	Biolegend	Cat# 344721; RRID: AB_2075390
Anti-human CD3 PE/Cyanine7	Biolegend	Cat# 300419; RRID: AB_439781
Anti-human IFNγ PE	Biolegend	Cat# 506506; RRID: AB_315440
Anti-PTEN	Cell Signaling Technology	Cat# 9559; RRID: AB_390810
Anti-β-actin	MBL	Cat# PM053-7; RRID: AB_10697035
Anti-HMGB1	Abcam	Cat# ab79823; RRID: AB_1603373
Anti-Galectin 1	Abcam	Cat# ab138513; RRID: AB_2894851
Anti-Flag tag (IF & PLA)	Proteintech	Cat# 80010-1-RR; RRID: AB_2882940
Anti-Flag tag	Sigma-Aldrich	Cat# A8592; RRID: AB_439702
Anti-V5 Tag	Abcam	Cat# ab182008
Anti-HSP90B1	Cell Signaling Technology	Cat# 20292; RRID: AB_2722657
Anti-HSP90AB1	Proteintech	Cat# 11405-1-AP; RRID: AB_2121207
Anti-GM130	Abcam	Cat# ab52649; RRID: AB_880266
Anti-Clusterin	Abcam	Cat# ab92548; RRID: AB_10585132
Anti-His Tag	Cell Signaling Technology	Cat# 12698; RRID: AB_2744546
Anti-HA Tag	Cell Signaling Technology	Cat# 3724; RRID: AB_1549585
Anti-HA Tag (PLA)	Cell Signaling Technology	Cat# 2367; RRID: AB_10691311
Anti-Phospho-AKT (Ser473)	Cell Signaling Technology	Cat# 4060; RRID: AB_2315049
Anti-AKT (pan)	Cell Signaling Technology	Cat# 4691; RRID: AB_915783
Anti-Flotillin 1	Proteintech	Cat# 15571-1-AP; RRID: AB_2106746

(*Continued on next page*)

Please cite this article in press as: Zhang et al., Secreted PTEN binds PLXDC2 on macrophages to drive antitumor immunity and tumor suppression, Developmental Cell (2024), https://doi.org/10.1016/j.devcel.2024.08.003

Continued

REAGENT or RESOURCE	SOURCE	IDENTIFIER
Anti-PLXDC2	Proteintech	Cat# 12285-1-AP; RRID: AB_2166239
Anti-JAK1	Cell Signaling Technology	Cat# 3344; RRID: AB_2265054
Anti-Phospho-JAK1 (Tyr1034/1035)	Cell Signaling Technology	Cat# 74129; RRID: AB_2799851
Anti-JAK2	Cell Signaling Technology	Cat# 3230; RRID: AB_2128522
Anti-Phospho-JAK2 (Tyr1008)	Cell Signaling Technology	Cat# 8082; RRID: AB_10949104
Anti-JAK3	Cell Signaling Technology	Cat# 8863; RRID: AB_11024093
Anti-Phospho-JAK3 (Tyr980/981)	Cell Signaling Technology	Cat# 5031; RRID: AB_10612243
Anti-TYK2	Proteintech	Cat# 16412-1-AP; RRID: AB_2918047
Anti-Phospho-TYK2 (Tyr1054)	Abmart	Cat# TA8002
Anti-STAT1	Cell Signaling Technology	Cat# 14994; RRID: AB_2737027
Anti-STAT2	Cell Signaling Technology	Cat# 72604; RRID: AB_2799824
Anti-STAT3	Cell Signaling Technology	Cat# 30835; RRID: AB_2798995
Anti-STAT4	Cell Signaling Technology	Cat# 2653; RRID: AB_2255156
Anti-STAT5	Cell Signaling Technology	Cat# 94205; RRID: AB_2737403
Anti-STAT6	Cell Signaling Technology	Cat# 5397; RRID: AB_11220421
Anti-Phospho-STAT1 (Tyr701)	Cell Signaling Technology	Cat# 7649; RRID: AB_10950970
Anti-Phospho-STAT2 (Tyr690)	Bioss	Cat# bs-3428R; RRID: AB_10882233
Anti-Phospho-STAT3 (Tyr705)	Cell Signaling Technology	Cat# 9145; RRID: AB_2491009
Anti-Phospho-STAT4 (Tyr693)	Abcam	Cat# ab28815; RRID: AB_2196601
Anti-Phospho-STAT5 (Tyr694)	Cell Signaling Technology	Cat# 4322; RRID: AB_10544692
Anti-Phospho-STAT6 (Tyr641)	Abcam	Cat# ab263947
Anti-Histone H3	Cell Signaling Technology	Cat# 4499; RRID: AB_10544537
Anti-β-tubulin	YEASEN	Cat# 30303ES50
InVivoMAb mouse IgG2a isotype control	Bio X Cells	Cat# BE0085; RRID: AB_1107771
InVivoMAb anti-mouse NK1.1	Bio X Cells	Cat# BE0036; RRID: AB_1107737
InVivoMAb rat IgG2b isotype control	Bio X Cells	Cat# BE0090; RRID: AB_1107780
InVivoMAb anti-mouse CD8a	Bio X Cells	Cat# BE0117; RRID: AB_10950145
InVivoMAb anti-mouse F4/80	Bio X Cells	Cat# BE0206; RRID: AB_10949019
InVivoMAb anti-mouse Ly6G/Ly6C (Gr- 1)	Bio X Cells	Cat# BE0075; RRID: AB_10312146
InVivoPlus rat IgG2a isotype control	Bio X Cells	Cat# BP0089; RRID: AB_1107769
InVivoPlus anti-mouse PD-1 (CD279)	Bio X Cells	Cat# BP0146; RRID: AB_10949053
Chemicals, peptides, and recombinant proteins		
Brefeldin A (BFA)	MCE	Cat# HY-16592
RIPA Lysis Buffer	Millipore	Cat# 20-188
JetPrime	Polyplus	Cat# 114-15
X-tremeGENE™ 9 DNA Transfection Reagent	Roche	Cat# 6365809001
Lipofectamine RNAiMAX Reagent	Invitrogen	Cat# 13778150
Anti-Flag M2 affinity Gel	Sigma-Aldrich	Cat# A2220: RRID: AB_10063035
Anti-HA Agarose	ThermoFisher Scientific	Cat# 26182; RRID: AB_2532162
HisSep Ni-NTA Agarose Resin	YEASEN	Cat# 20502ES50
Collagenase type IV	Sigma-Aldrich	Cat# C4-22-1G
Collagenase type II	Sigma-Aldrich	Cat# C2-22-1G
DNase I	Roche	Cat# 11284932001
Intracellular Fixation & Permeabilization Buffer Set	eBioscience	Cat# 88-8824-00
Zombie NIR™ Fixable Viability Kit	Biolegend	Cat# 423106
Cell Stimulation Cocktail (plus protein transport inhibitors)	eBioscience	Cat# 00-4975-03

(*Continued on next page*)

Please cite this article in press as: Zhang et al., Secreted PTEN binds PLXDC2 on macrophages to drive antitumor immunity and tumor suppression, Developmental Cell (2024), https://doi.org/10.1016/j.devcel.2024.08.003

Continued

REAGENT or RESOURCE	SOURCE	IDENTIFIER
Flag tag peptide	Sigma-Aldrich	Cat# F3290
Recombinant murine M-CSF	Sino Biological	Cat# 51112-MNAH
Recombinant murine IFNγ	PeproTech	Cat# 315-05
Recombinant murine IL-4	Biolegend	Cat# 715004
Recombinant murine IL-13	MCE	Cat# HY-P70460
Recombinant Murine IL-15	PeproTech	Cat# 210-15
Recombinant murine IL-12	MCE	Cat# HY-P73159
Recombinant murine IL-18	MCE	Cat# HY-P70642AF
SuperGrow® Cell Culture Supplemental Mix	DAKEWE	Cat# 6122012
Recombinant PTEN	This paper	N/A
Recombinant PTEN-C124S	This paper	N/A
Recombinant PTEN-W274L	This paper	N/A
Recombinant PTEN-V275L	This paper	N/A
Recombinant His-SUMO-TMED10	This paper	N/A
Recombinant PLXDC2-ECD (aa31-455)	MCE	Cat# HY-P71215
Recombinant PLXDC2-ICD (aa477-530)	This paper	N/A
JAK2-IN-6	MCE	Cat# HY-137756
Z3	MCE	Cat# HY-15480
Fludarabine	MCE	Cat# HY-B0069
Critical commercial assays		
PTEN ELISA Kit	Abcam	Cat# ab206979
Duolink In Situ Red Starter Kit	Sigma-Aldrich	Cat# DUO92101
NE-PER Nuclear and Cytoplasmic Extraction Reagents	ThermoFisher Scientific	Cat# 78835
MojoSort™ Mouse CD8 T Cell Isolation Kit	BioLegend	Cat# 480008
MojoSort™ Mouse NK Cell Isolation Kit	BioLegend	Cat# 480050
MojoSort™ Human CD8 T cell Isolation Kit	BioLegend	Cat# 480012
MojoSort™ Human NK Cell Isolation Kit	BioLegend	Cat# 480054
CD3/CD28 Streptamer® Kit, mouse	IBA Life Sciences	Cat# 6-8920-050
Human T cell Activation/Expansion CD3/CD28 Beads	ACROBiosystems	Cat# MBS-C001
Natural Killer Cells Induction Culture Kit	DAKEWE	Cat# 6813523
Deposited data		
Data files for B16-F10-ΔPTEN tumors RNA-seq	This paper	GEO: GSE249142
Data files for scRNA-seq from B16-F10-ΔPTEN tumors	This paper	GEO: GSE249052
Data files for BMDMs RNA-seq	This paper	GEO: GSE249577
Original images of Western blot	This paper; Mendeley Data	https://doi.org/10.17632/6c4cdk9yzr.1
Experimental models: Cell lines		
293T	Cell Bank of Chinese Academy of Sciences	Cat# GNHu17
B16-F10	Cell Bank of Chinese Academy of Sciences	Cat# TCM36
MC38	FuHeng	Cat# FH0125
CT26	Cell Bank of Chinese Academy of Sciences	Cat# TCM37
LLC	Cell Bank of Chinese Academy of Sciences	Cat# TCM 7
Experimental models: Organisms/strains		
Mouse: NCG	GemPharmatech	Strain# T001475
Mouse: C57BL/6J-*Plxdc2*$^{fl/fl}$	GemPharmatech	Strain# T021699

(*Continued on next page*)

Please cite this article in press as: Zhang et al., Secreted PTEN binds PLXDC2 on macrophages to drive antitumor immunity and tumor suppression, Developmental Cell (2024), https://doi.org/10.1016/j.devcel.2024.08.003

Continued

REAGENT or RESOURCE	SOURCE	IDENTIFIER
Mouse: C57BL/6J-*Lyz2*-Cre	GemPharmatech	Strain# T003822
Oligonucleotides		
See Tables S4 and S5 for a detailed primers list	This paper	N/A
Recombinant DNA		
pLVX-IRES-PURO-TMED10-V5	This paper	N/A
pLVX-IRES-PURO-TMED10-3Flag	This paper	N/A
pET28a-TMED10	This paper	N/A
pQCXIN-3Flag-PTEN	This paper	N/A
pLVX-IRES-PURO-PTEN	This paper	N/A
pLVX-IRES-PURO-PTEN-HA	This paper	N/A
pGEX6p-1-PTEN	This paper	N/A
pET28a-PLXDC2-ICD	This paper	N/A
pEGFP-N1-ERGIC53	This paper	N/A
pEnCMV-JAK2-3FLAG	This paper	N/A
pLVX-IRES-PURO-PLXDC2-HA	This paper	N/A
Software and algorithms		
FlowJo	BD Biosciences	https://www.flowjo.com/
GraphPad Prism	GraphPad	https://www.graphpad.com/

RESOURCE AVAILABILITY

Lead contact

Further information and requests for resources and reagents should be directed to and will be fulfilled by the lead contact, Shao-Ming Shen (smshen@shsmu.edu.cn).

Materials availability

All the materials generated and used in this study will be available upon request.

Data and code availability

The RNA-seq and scRNA-seq datasets have been deposited at GEO and are publicly available as of the date of publication. Accession numbers are listed in the key resources table. The original Western blot images have been deposited at Mendeley and are publicly available as of the date of publication. The DOI is listed in the key resources table. This paper does not report original code. Any additional information required to reanalyze the data reported in this paper is available from the lead contact upon request.

EXPERIMENTAL MODEL AND STUDY PARTICIPANT DETAILS

Cell lines

293T, B16-F10 and MC38 cells were cultured in DMEM medium containing 10% FBS. LLC cells were cultured in DMEM-F12 medium containing 10% FBS. CT26 cells were cultured in RPMI 1640 medium containing 10% FBS. All the cells were cultured under 37 °C, 5% CO_2 condition. No signs of mycoplasma contamination were found for all cell lines. Short tandem repeat profiling was used for cell line authentication.

Mice

C57BL/6J and BALB/c mice were purchased from Shanghai Laboratory Animal Center, Chinese Academy of Sciences, and NCG mice were purchased from GemPharmatech. *Plxdc2*$^{fl/fl}$ mice and *Lyz2*-Cre mice on the C57BL/6J background were obtained from GemPharmatech. *Plxdc2*$^{fl/fl}$ × *Lyz2*-Cre mice were generated by crossing the *Plxdc2*$^{fl/fl}$ mice with *Lyz2*-Cre mice. All mouse protocols and experiments were in agreement with all of the animal research-related ethical regulations under the approval of the committee for humane treatment of animals at Shanghai Jiao Tong University School of Medicine (SJTU-SM). All mice used in our experiments were between 6 and 8 weeks of age, and were housed under SPF facilities at SJTU-SM. C57BL/6J mice were used for B16-F10 model, MC38 model and LLC model. BALB/c mice were used for CT26 model. NCG mice were used for B16-F10 model.

Please cite this article in press as: Zhang et al., Secreted PTEN binds PLXDC2 on macrophages to drive antitumor immunity and tumor suppression, Developmental Cell (2024), https://doi.org/10.1016/j.devcel.2024.08.003

Human samples

Tumor tissues and peripheral blood were collected from CRC patients with informed written consent, and under approval of local medical ethnics from Ruijin Hospital Affiliated to SJTU-SM and Renji Hospital Affiliated to SJTU-SM.

METHOD DETAILS

Western blot (WB)

Protein extracts were separated by SurePAGE (GenScript). After separation, proteins were transferred to nitrocellulose membrane (Bio-Rad), blocked by 5% nonfat milk for 1 h at room temperature and sequentially incubated in primary antibody in 2% BSA overnight at 4 °C. The following day, blots were washed in TBST and incubated in horseradish peroxidase (HRP)-linked secondary antibody (Cell Signaling) in 2% BSA for 1 h at room temperature. Immobilon Western Chemiluminescent HRP substrate kit (Millipore) was used for detection.

Plasmids, shRNA, sgRNA and lentiviruses

Information on the plasmids is provided in the key resources table, while information on the shRNA and sgRNA sequences is provided in Table S4. Lentivirus was produced by co-transfecting 293T cells with the lentiviral construct pCMV-dR8.91 (Δ8.9) plasmid and the pMDG envelope-expressing plasmid, using X-tremeGENE 9 DNA Transfection Reagent (Roche). Viral supernatant was harvested at 24-48 h post-transfection, passed through a 0.45 μm filter, and used to infect the target cells.

Secretion determination

For determination of protein secretion, cells were replaced with serum-free conditioned medium (SFCM) for 1 h. The SFCM was filtered through a 0.22 μm filter before being concentrated by a 10 kD Amicon filter (Millipore) and whole cell lysate (WCL) was collected. WB was performed to determine the indicated proteins in SFCM and WCL.

Immunoprecipitation (IP) and pull-down

For co-IP, the cells were lysed on ice for 30 min in RIPA buffer (Millipore) with protease inhibitor cocktail, and the lysates were cleared by centrifugation. The resulting supernatants were incubated with indicated agaroses and rotated at 4 °C for 2 h. Then the precipitates were washed four times with RIPA buffer, boiled in sample buffer and subjected to WB analysis.

For pull-down, the proteins were purified and the Flag-tagged bait was incubated with anti-Flag agarose (which was blocked by 5% milk) in RIPA buffer used for co-IP, and rotated at 4 °C for 1 h. Then the beads loaded with the bait were collected and incubated with the prey protein at 4 °C for 2 h. The beads were washed five times followed by WB analysis.

Duolink PLA

Duolink PLA kit was purchased from Sigma-Aldrich and the assay was performed according to the product manual. In brief, PTEN-HA and TMED10-Flag were expressed in ERGIC53-GFP-expressing PTEN-knockout 293T cells. The cells were fixed with 4% paraformaldehyde for 15 min and permeabilized with 0.1% Triton X-100 diluted in PBS at room temperature. The cells were blocked, incubated with primary antibodies and PLA probes followed by ligation and amplification using the recommended conditions according to the manual.

Protein expression and purification

PTEN or its derivatives were inserted into a GST fusion expression vector pGEX6p-1. TMED10 and PLXDC2-ICD were cloned into the pET28a vector. PTEN, TMED10 and PLXDC2-ICD were individually expressed in *Escherichia coli* BL21 (DE3) (YEASEN), and were purified with glutathione sepharose 4B beads (GE Healthcare) or HisSep Ni-NTA Agarose Resin (YEASEN) in lysis buffer (25 mM Tris-HCl, pH 8.0, 500 mM NaCl, 10% glycerol) with protease inhibitor cocktail. The GST tag was removed through protease 3C digestion. The proteins were further purified by gel-filtration chromatography equilibrated with PBS containing 1 mM DTT. The purified proteins were concentrated with an Amicon filter (Millipore), then stored in aliquots at - 80 °C.

CRISPR-mediated knockout

For the generation of PTEN-knockout cell lines, the indicated cells were transfected with the plasmid containing CAS9 and sgRNA. Puromycin was used to select positive cells. Then the cells were diluted and single colonies were isolated. The effect of sgRNA was detected by WB. PCR and sequencing were used to confirm homozygous editing of the gene loci.

Tumor treatment experiments

For B16-F10 model, 1.0×10^5 cells were subcutaneously injected into C57BL/6J or NCG mice. For LLC and MC38 models, 1.0×10^5 cells were subcutaneously injected into C57BL/6J mice. For CT26 model, 1.0×10^5 cells were subcutaneously injected into BALB/c mice. Treatments were given as single agents or in combination, with the following regimen for each drug. For PTEN treatment, once tumors reached ~ 50-100 mm^3 in volume, mice were randomly assigned to control or treatment groups and were intratumorally or intraperitoneally injected with PTEN proteins or PBS every day. Unless specified, 10 μg PTEN was used for each injection. For PLXDC2-ECD treatment, once tumors reached ~ 50-100 mm^3 in volume, mice were randomly assigned to control or treatment groups and were intratumorally injected with PLXDC2-ECD alone or PLXDC2-ECD with PTEN proteins at a ratio of 10:1 every day. For immune

Please cite this article in press as: Zhang et al., Secreted PTEN binds PLXDC2 on macrophages to drive antitumor immunity and tumor suppression, Developmental Cell (2024), https://doi.org/10.1016/j.devcel.2024.08.003

checkpoint blockade treatment, once tumors reached ~ 50-100 mm^3 in volume, mice were randomly assigned to control or treatment groups and were intraperitoneally injected with anti-PD-1 antibodies (10 mg /kg, RMP1-14, Bio X Cells) or isotypes (10 mg /kg, 2A3, Bio X Cells). Antibody treatments were conducted every 2 days. For *in vivo* macrophage adoptive transfer experiments, B16-F10-ΔPTEN cells were subcutaneously co-injected with BMDMs transduced with shNC or PLXDC2-targeted shRNAs at a ratio of 1:5 into C57BL/6J mice. Tumor size was measured by calipers, and the volume was calculated using length × $(width)^2$ /2.

Cell isolation

Mouse tumor samples were cut into 1 mm^3 pieces with scissors and subjected to enzymatic digestion with collagenase type IV (2 mg/mL) and DNase I (1 mg/mL) in DMEM for 1 h at 37 °C. Mouse spleens were minced and digested with collagenase type II (250 μg/mL) and DNase I (1 mg/mL) at 37 °C for 30 min. After treatment with red blood cell lysis buffer for 5 min at room temperature, all samples were washed and re-suspended in flow cytometry buffer (PBS containing 1% FBS) or DMEM depending on further use.

Flow cytometry staining and analysis

Live single cells were sub-gated by staining with Zombie NIR™ (Biolegend) for 15 min. For blocking of Fc receptors, cells were then pre-incubated with anti-CD16/32 antibodies (Biolegend) for 10 min on ice before immunostaining. After one wash with flow cytometry buffer, cells were incubated with appropriate dilutions of various combinations of the following antibodies. Primary antibodies to cell surface markers directed against CD45, CD3, CD8a, CD4, NK1.1, CD49b, CD11b, F4/80, Ly6G, CD14, CD86 and CD56. For intracellular staining, cells were fixed, permeabilized using Intracellular Fixation & Permeabilization Buffer Set (eBioscience), and then stained with antibodies to CD206. For cytokine staining, cells were first stimulated with Cell Stimulation Cocktail (eBioscience) at 37 °C for 4 h, and then stained with anti-IL-1β, anti-IFNγ or anti-Granzyme A antibodies. The stained cells were acquired by a Beckman CytoFlex S Flow Cytometer, and data generated were processed using FlowJo software.

Bone marrow-derived macrophages (BMDMs) polarization and stimulation

To obtain the bone marrow-derived macrophages (BMDMs), bone-marrow (BM) cells were harvested from femurs and tibia of C57BL/6J mice. Differentiation was induced by recombinant M-CSF (50 ng/mL, Sino Biological) in DMEM medium (Gibco) containing 10% FBS and 1% penicillin/streptomycin for 7 days. The attached cells at the end of the culture are naive macrophages (M0-like). Then the cells were washed and cultured in DMEM medium described above but without M-CSF for subsequential treatments. To polarize macrophages toward an M1-like phenotype, we stimulated BMDMs with IFNγ (20 ng/mL, PeproTech) for 48 h. To induce an M2-like phenotype, we treated BMDMs with IL-4 (10 ng/mL, Biolegend) and IL-13 (10 ng/mL, MCE) for 48 h. To stimulate BMDMs with PTEN, we cultured BMDMs with 100 ng/mL PTEN for 24 or 48 h. To stimulate BMDMs with tumor-cell-conditioned medium (TCM), we cultured BMDMs with complete medium containing 50% TCM (volume) for 48h.

RNA sequencing (RNA-seq) and analysis

RNA-Seq was performed by Shanghai Personal Biotechnology (Shanghai, China). RNA-seq reads were aligned with HISAT2 (v.2.2.1) using the default parameters to the Mus musculus reference genome Mus_musculus.GRCm38. SAM files were converted to BAM and sorted using samtools (v.1.6). Count matrices were generated using featureCounts (v.2.0.1) with the GENCODE.vM23. R (v.4.2.3) package DESeq2 (v.1.38.0) was used for data normalization, analysis of differentially expressed genes (DEGs) and principal component analysis. Normalized values were used for scatterplot and heatmap.

Patient clinical information and gene expression was downloaded and extracted from TCGA database (https://portal.gdc.cancer.gov). We first estimated the proportions of $PLXDC2^+$ and $PLXDC2^-$ TAMs in individual samples through cell deconvolution analysis using Cibersort R script with the parameter perm = 1000 and QN = F. The customized cell-type-specific signature genes were created by the creation feature of CIBERSORTx (https://cibersortx.stanford.edu). The fragments per kilobase of transcript per million mapped reads (FPKM) values of individual samples as a mixture file. For survival analysis, the patients were divided into two groups: high or low proportions of $PLXDC2^+$ TAMs. The cumulative event (death) rate was calculated for each patient group using the Kaplan–Meier method, and the survival curves of the two patient groups were compared using the Kaplan–Meier (log rank) test.

Single-cell RNA sequencing (scRNA-seq) and analysis

scRNA-seq was performed by Shanghai Personal Biotechnology (Shanghai, China). CellRanger (v.7.0.0) was used to align reads to Cell Ranger reference package refdata-gex-mm10-2020-A. Gene expression was analyzed using Seurat (v.4.1.1).[21] Cells with <5% mitochondrial content and >200 and <8200 detected genes were considered. Mitochondrial content was regressed out during SCT normalization. We used the SelectIntegrationFeatures function in Seurat to select the 3000 variable genes to be integrated and used FindNeighbors and FindCluster in Seurat to obtain cell clusters. The cell clustering analysis stage classified cells into cancer cells, fibroblasts, macrophages, neutrophils, DC cells, T cells, and B cells. Cellular annotation was performed manually by examining the highest expressed marker genes between clusters corresponding to cellular markers provided in the literature and databases, including macrophages (Cd86, Csf1r, Mertk), neutrophils (S100a8, S100a9), DC cells (H2-Aa, H2-Ab1), T cells (Cd3e, Cd4, Cd8a), B cells (Cd19, Cd79a) and fibroblasts (Dcn). The AddModuleScore function in Seurat calculates M1-like and M2-like macrophage cell expression-based scores. The lists of M1 and M2 cell type-specific gene markers are summarized as follows: M1 (Lcn2, Tnfaip2, Lyz2, Fth1, Il1r1, Nos2, Tlr2, Tlr4, Il1b, Il18, Il12b, Il6, Cxcl2, Ifng, Cd38, Tnf, Socs3, Ptgs2, Nfkbiz, Lrf5, Gpr18, Fpr2, Cxcl10, Azin1, Cd68, Ccl5, Irf1, Irf5, Il1a, Ido1, Il12a and Il23a) and M2 (Myc, Cd83, Mrc1, Arg1, Egr2, Ccr7, Chil4, Pparg, Cd163, Clec7a, Il10, Il4,

Please cite this article in press as: Zhang et al., Secreted PTEN binds PLXDC2 on macrophages to drive antitumor immunity and tumor suppression, Developmental Cell (2024), https://doi.org/10.1016/j.devcel.2024.08.003

Irf4, Pdgfb, Stat6, Chil3, Cd40, Csf1, Tlr7, Ccl13, Ccl17, Ccl18, Ccl22, Ccl24, Cd86, Vegfa, Vegfb, Vegfc, Vegfd, Mmp9, Fn1, Egf, Lyve1, Mmp14, Mmp19, Cd276, Fasl, Ctsa, Ctsb, Ctsc, Ctsd, Mgl2, Ear11, Clec10a, Retnla and Ccl10).

A scRNA-seq dataset (accession ID: GSE178341, human CRC; GSE151530, human liver cancer; GSE160269, human ESCC) that was previously reported was obtained from the Gene Expression Omnibus (GEO) (https://www.ncbi.nlm.nih.gov/geo/) database. From the three datasets, we collected unique molecular identifier (UMI) count matrix for cells selected based on the quality control criteria as well as the cell type annotations reported in the original study. Only the UMI count profiles for 40757 cells corresponding to TAMs (GSE178341, 20411 cells; GSE160269, 5174 cells; GSE151530, 14260 cells) were used for our analysis. To merge samples and reduce batch effect, each sample was normalized using Seurat (v5.1.0) SCT transformation pipeline. Clusters were identified with the Seurat functions FindNeighbors and FindClusters. We then visualized the resulting subclusters of TAMs using uniform manifold approximation and projection (UMAP) with the RunUMAP function in Seurat. Genes predominantly upregulated in each subcluster were identified using the FindAllMarkers function with an adjusted P value of < 0.05 and $\log_2$-fold change of > 0.25. To identify the PLXDC2$^+$/ PLXDC2$^-$ TAMs in these cells, PLXDC2 expression was categorized into the following three groups: (1) high enrichment of PLXDC2 expression, (2) low enrichment of PLXDC2 expression, and (3) no expression of PLXDC2. Of these groups, we focused on (1) high enrichment of PLXDC2 expression group, with significant numbers of both PLXDC2$^+$ and PLXDC2$^-$ TAMs, for a fair comparison between the two cell types.

Cell interaction analysis

CellChat (v 1.5.0) was used to infer and compare intercellular communication between cell types and conditions. A CellChat object was created with our scRNA-seq data cells grouped by their cluster labels to infer cell communication between clusters. The CellChat-curated mouse ligand receptor database was used to validate the molecular interactions in the dataset. CellChat computes probabilities for biologically significant communication patterns by assessing and integrating gene expression levels along with prior known knowledge for molecular interactions. Bubble plots were created based on the communication probabilities computed for ligand receptor pairs by CellChat's algorithm.

GO Term and Gene Set Enrichment Analysis (GSEA)

Gene Ontology (GO) enrichment analysis were performed using the DAVID website (https://david.ncifcrf.gov), with DEGs by DESeq2 (FC > 2.5 or < 0.4 with P value < 0.05) used as input. GSEA analysis for RNA-seq was performed using JavaGSEA (v.4.3.2).

RT-qPCR

Total RNA from indicated cells was extracted with Trizol (Invitrogen) according to the manufacturer's protocol. RNA was digested with DNase I (Promega), reverse transcribed to cDNA using random primers (Takara) and M-MLV Reverse Transcriptase (Promega), followed by RT-qPCR with the SYBR Green PCR Master Mix (Applied Biosystems). Expression levels of target genes were normalized to the expression of *Rpl13a* (internal control) and calculated based on the comparative cycle threshold (CT) method ($2^{-\Delta\Delta CT}$). The primers used are listed in Table S5.

Enzyme-linked immunosorbent assay (ELISA)

The levels of extracellular PTEN in cell culture supernatant, tumor interstitial fluid (TIF), lymphoid nodes or blood were detected by PTEN ELISA kits (Abcam) according to the manufacturer's instructions.

Mass cytometry (CyTOF) and data analysis

Tumor tissue was cut into 1mm^3 pieces and then subjected to digestive enzyme mix (Miltenyi). Incubate the tissue soup in a shaking incubator at 37 °C for 1 h. Filter the dissociated tissue through the 40 μm cell strainer. Cells were collected by centrifugation and resuspended. Cells were washed once with PBS and then stained with 100 μL of 250 nM cisplatin (Fluidigm) for 5 min on ice to exclude dead cells, and then incubated in Fc receptor blocking solution before stained with surface antibodies cocktail for 30 min on ice. Cells were washed twice with FACS buffer and fixed in 200 μL of intercalation solution (Maxpar Fix and Perm Buffer containing 250 nM 191/193Ir, Fluidigm) overnight. After fixation, cells were washed once with FACS buffer and then perm buffer (eBioscience), stained with intracellular antibodies cocktail for 30 min on ice. Cells were washed and resuspend with deionized water, adding into 20% EQ beads (Fluidigm), acquired on a mass cytometer (Helios, Fluidigm). Antibody clones are listed in Table S6.

Data of each sample were debarcoded from raw data using a doublet-filtering scheme with unique mass-tagged barcodes. Each .fcs file generated from different batches were normalized through bead normalization method. Manually gate data using a FlowJo software to exclude to debris, dead cells and doublets, leaving live, single immune cells. Apply the X-shift clustering algorithm to all cells to partition the cells into distinct phenotypes based on marker expression levels. Annotate cell type of each cluster according to its marker expression pattern on a heatmap of cluster vs marker. Use the dimensionality reduction algorithm t-SNE to visualize the high-dimensional data in two dimensions and show distribution of each cluster and marker expression and difference among each group or different sample type. Perform t-test statistical analysis on the frequency of annotated cell population.

siRNA knockdown studies

BMDMs were transfected with negative control siRNA (siNC) or PLXDC2 siRNA using Lipofectamine RNAiMAX Transfection Reagent in Opti-MEM™ I reduced serum medium according to the manufacturer's protocol (ThermoFisher Scientific). Knockdown efficiency and subsequent experiments were performed 48-72 h post transfection. The information on the siRNA sequences is provided in Table S4.

Please cite this article in press as: Zhang et al., Secreted PTEN binds PLXDC2 on macrophages to drive antitumor immunity and tumor suppression, Developmental Cell (2024), https://doi.org/10.1016/j.devcel.2024.08.003

Purification of tumor-associated macrophages (TAMs) from human tumor samples

Human tumor samples were chopped with scissors and then subjected to digestive enzyme mix (Absin) for 1 h at 37 °C. Next, tissues were filtered through 40 μm cell strainer to achieve single-cell suspensions. Single cells were then stained with Zombie NIR™ (Biolegend) to exclude dead cells, and anti-CD45 (HI30, Biolegend), anti-CD11b (ICRF44, Biolegend) and anti-CD14 (M5E2, Biolegend) for flow sorting on a FACSAria III Cell Sorter (BD Biosciences). To stimulate tumor-associated macrophages (TAMs) with PTEN, we cultured TAMs with 100 ng/mL PTEN for 24 or 48 h.

Macrophage depletion

Macrophages were depleted by intraperitoneal injection of anti-mouse F4/80 antibodies (clone CI:A3-1, Bio X Cells) (200 μg/injection) on day - 3, + 1, + 3, + 5 and + 7 with respect to tumor cell injection. Macrophages depletion was confirmed by flow cytometry.

Neutrophil depletion

Anti-mouse Ly6G antibodies (clone RB6-8C5, Bio X Cells) or rat IgG2b (isotype control, Bio X Cells) were intraperitoneally injected (12.5 μg/injection), 3 days prior to B16-F10 cell injection and every day after injection. Neutrophils depletion was confirmed by flow cytometry.

$CD8^+$ T cell depletion

Anti-mouse CD8a antibodies (clone YTS 169.4, Bio X Cells) or rat IgG2b (isotype control, Bio X Cells) were intraperitoneally injected (200 μg/injection) 3 days before B16-F10 cell injection, and three times/week after injection. $CD8^+$ T cell depletion was confirmed by flow cytometry.

NK cell depletion

Anti-mouse NK1.1 antibody (clone PK136, Bio X Cells) or IgG2a (isotype control, Bio X Cells) were intraperitoneally injected (200 μg/injection) 3 days before B16-F10 cell injection, and three times/week after injection. NK cell depletion was confirmed by flow cytometry.

Immunofluorescence (IF)

The indicated naive or M2-polarized BMDMs were treated with Flag or PTEN-Flag for 1 h, and subjected to immunofluorescent staining of Flag-tag following the steps below. The cells were washed once with PBS and immediately incubated with 4% paraformaldehyde for 15 min at room temperature. The cells were further blocked with 2% BSA diluted with PBS for 1 h and primary antibody incubation overnight at 4 °C. The cells were washed three times with PBS, followed by secondary antibody incubation for 1 h at room temperature. Fluorescence images were acquired using the Leica TCS SP8.

In vitro co-culture with $CD8^+$ T cells or NK cells

Spleens from wild-type C57BL/6J mice were harvested and filtered through a 40 μm cell strainer to generate a single-cell suspension. Mouse $CD8^+$ T cells and NK cells were isolated with MojoSort™ Mouse CD8 T Cell Isolation Kit (BioLegend) and MojoSort™ Mouse NK Cell Isolation Kit (BioLegend). The purity of the isolated cells was evaluated by flow cytometry. Mouse $CD8^+$ T cells were counted and cultured in the RPMI 1640 medium containing 10% FBS, 1% penicillin/streptomycin and 50 mM β-mercaptoethanol, and activated with CD3/CD28 Streptamer® Kit (IBA Life Sciences). Mouse NK cells were cultured in the RPMI 1640 medium containing 10% FBS, 1% penicillin/streptomycin and IL-15 (10 ng/mL; Peprotech). On day 6, Mouse NK cells were activated with IL-12 (25 ng/mL; MCE), IL-15 (50 ng/mL) and IL-18 (5 ng /mL; MCE) for 24 h.

Human peripheral blood mononuclear cells (PBMCs) were isolated from human peripheral blood by Ficoll (Cytiva) density gradient centrifugation. Human $CD8^+$ T cells and NK cells were isolated from PBMCs with MojoSort™ Human CD8 T cell Isolation Kit (BioLegend) and MojoSort™ Human NK Cell Isolation Kit (BioLegend). The purity of the isolated cells was evaluated by flow cytometry. Human $CD8^+$ T cells were cultured in the RPMI 1640 medium containing 10% FBS, 1% penicillin/streptomycin, and activated with ActiveMax® Human T cell Activation/Expansion CD3/CD28 Beads (ACROBiosystems). The sorted human NK cells were cultured using Natural Killer Cells Induction Culture Kit (DAKEWE) with 10% SuperGrow® Cell Culture Supplemental Mix (DAKEWE) and 1% penicillin/streptomycin.

To educate the macrophages, we cultured BMDMs or human tumor-associated macrophages (TAMs) with 100 ng/mL PTEN for 24 or 48 h. Macrophages were seeded with activated $CD8^+$ T cells or NK cells at a ratio of 5:1. After co-culture for 24 h, $CD8^+$ T cells or NK cells were collected for flow cytometry analysis.

QUANTIFICATION AND STATISTICAL ANALYSIS

The data statistic was performed using Prism software. The statistical information of each experiment, including the statistical methods, the *P* values and numbers (n), were shown in the figures and corresponding legends.